REPORT DOCUMENTATION PAGE

Form Approved OMB No. 074-0188

1. REPORT DATE *(DD-MM-YYYY)*	2. REPORT TYPE	3. DATES COVERED *(From – To)*
28-02-2007	Final report	June 15, 2001 – August 31, 2006

4. TITLE AND SUBTITLE

Analysis and Design of Ultrawide-Band and High-Power Microwave Pulse Interactions with Electronic Circuits and Systems

5a. CONTRACT NUMBER
NA

5b. GRANT NUMBER
F49620-01-1-0436

5c. PROGRAM ELEMENT NUMBER
NA

6. AUTHOR(S)

Uslenghi, Piergiorgio L. E. (PI)
Erricolo, Danilo (Co-PI)
Yang, Hung-Yu D. (Co-PI)

5d. PROJECT NUMBER
NA

5e. TASK NUMBER
NA

5f. WORK UNIT NUMBER
NA

7. PERFORMING ORGANIZATION NAMES(S) AND ADDRESS(S)

University of Illinois at Chicago
Dept. of ECE (MC 154)
851 South Morgan Street, Chicago, IL 60607-7053

8. PERFORMING ORGANIZATION REPORT NUMBER

NA

9. SPONSORING/MONITORING AGENCY NAME(S) AND ADDRESS(ES)

Air Force Office of Scientific Research
875 N. Randolph Street – Suite 325
Arlington, VA 22203-1768

Dr Ryan Umstattel/NE

10. SPONSOR/MONITOR'S ACRONYM(S)
NA

AFRL-SR-AR-TR-07-0139

12. DISTRIBUTION/AVAILABILITY STATEMENT

APPROVED FOR PUBLIC RELEASE; DISTRIBUTION UNLIMITED.

13. SUPPLEMENTARY NOTES

This report and most of related research publications are available on the Web at: www.ece.uic.edu/MURI-RF.

The results under this grant are the coordinated effort of researchers at six universities: University at Illinois at Chicago, Clemson University, Ohio State University, University of Houston, University of Michigan, and University of Illinois at Urbana-Champaign.

14. ABSTRACT

This research is directed to understanding and modeling the effects of electromagnetic pulse interactions with electronic circuits and systems, and is focused on four major tasks. (1) Characterization of coupling mechanisms responsible for guiding electromagnetic energy from the source to the electronic components, via topology schemes based on a generalized scattering matrix. Frequency-domain and time-domain solvers are developed for large-scale systems. The results are validated via measurements and via comparison with new canonical solutions to scattering and penetration problems. (2) Characterization of the spurious waveforms at the input ports of the electronic systems. A full-wave three-dimensional analysis of linear passive systems is developed to convert the radiating and conducting EMI into sets of noise sources at the ports of nonlinear active circuits. A network-oriented nonlinear transient simulator is developed for small-signal and large-signal analysis of nonlinear electronics, including the distributed nature of the coupling path and EMI sources. (3) Determination of conditions for induced change-of-logic states and alterations of logic functions for digital circuits and computer systems. A fault-tolerance analysis is developed to determine, classify, monitor and control various system program errors under EM threat. (4) Experiments to validate EM penetration and coupling predictions, and circuit and system fault models.

15. SUBJECT TERMS

Electromagnetic interference. Ultrawide-band pulses. High-power microwave pulses. Interactions with electronic circuits and systems.

16. SECURITY CLASSIFICATION OF:			17. LIMITATION OF ABSTRACT	18. NUMBER OF PAGES	19a. NAME OF RESPONSIBLE PERSON
a. REPORT	b. ABSTRACT	c. THIS PAGE			Piergiorgio L. E. Uslenghi
U	U	U	UU	54	19b. TELEPHONE NUMBER *(Include area code)* 312-996-6059; fax: 312-996-8664; email: uslenghi@uic.edu

Standard Form 298 (Rev. 8-98)
Prescribed by ANSI Std. Z39-18

Final Performance Report

AFOSR-MURI F49620-01-0436

Analysis and design of ultra wide-band and high-power microwave pulse interactions with electronic circuits and systems

PI: Prof. Piergiorgio L.E. Uslenghi, University of Illinois at Chicago

Team members:

University of Illinois at Chicago
- **Prof. Shantanu Dutt**
- **Prof. Danilo Erricolo**
- **Prof. H.Y. David Yang**

Clemson University
- **Prof. Michael A. Bridgwood**
- **Prof. Chalmers M. Butler**
- **Prof. Anthony Q. Martin**
- **Prof. Frederick M. Tesche**

University of Houston
- **Prof. Donald R. Wilton**
- **Prof. David R. Jackson**

Ohio State University
- **Prof. John L. Volakis**

University of Illinois at Urbana Champaign
- **Prof. Andreas C. Cangellaris**

University of Michigan
- **Prof. Pinaki Mazumder**
- **Prof. Eric Michielssen**
- **Prof. V. V. Liepa**

Report Period: June 15, 2001 to August 31, 2006

PROJECT SUMMARY

Ultra wide-band (UWB) environments and narrow-band, high power microwave (HPM) sources present inadvertent or deliberate threats to communication systems, computers, vehicles, or security systems. The fact that the operating frequency spectra of those sources extend well beyond several GHz in conjunction with the ever-changing sophistication of digital circuits presents new technological challenges for the understanding, analysis, modeling, and design of the overall impact. In microwave regimes and above, conventional radio frequency (RF) electronic devices are comparable to a wavelength and become distributed circuits. Moreover, small apertures or cracks on the system shielding are no longer negligible and may become the salient features of the whole structure. Strong electromagnetic coupling between various components as well as shielding cavity resonances further complicates the physics of the UWB and HPM effects on electronics. There is an urgent need to understand and model the effects of UWB and HPM interactions with electronic circuits and systems at all scales. In this MURI project, we developed new technology essential for accurately assessing, analyzing, computing, and designing UWB and HPM coupling into sophisticated electronic systems. **Our efforts included four major tasks. (1) Characterization of coupling mechanisms responsible for guiding electromagnetic (EM) energy from the source/generators down to electronic components, with highly advanced frequency-domain and time-domain hybrid EM solvers for large-scale systems developed though out this project.** Through the use of EM topology schemes, the EM coupling of pieces is included with a generalized scattering matrix analysis. Proper transfer functions were developed for each coupling component. **(2) Characterization of the spurious waveforms at the chip or digital electronics from the penetrated HPM/UWB sources.** A full-wave three-dimensional EM analysis of linear passive systems is developed successfully to convert the radiating and conducting EMI into sets of noise sources at the input ports of nonlinear active circuits. Electrical circuit models for coupling paths (traces, interconnects, and linear passive components) were also developed with full-wave EM solvers. A network-oriented nonlinear transient simulator was developed for small-signal and large-signal analysis of nonlinear electronics, including the distributed nature of the coupling path and EMI sources. **(3) Determination of conditions for induced change-of-logic states and alterations of logic functions for digital circuits and computer systems.** The fault-tolerance analysis was used to determine, classify, monitor and control various system program errors under EM threat. **(4) System, subsystem and component design and testing with experiments for the validation of EM penetration and coupling and circuit and system fault models.**

Our MURI team consists of fifteen faculty members from six major research universities with multi-disciplinary expertise and leadership on large-scale EM modeling, EMI/EMP on circuits and systems, microwave integrated circuit modeling, designs of VLSI and digital circuits and systems, computer-system fault analysis, and EMI/EMP testing. Through this MURI project, our multi-disciplinary team has successfully pushed existing EMI/EMC technology into much higher frequency regimes for UWB and HPM sources.

The major contributions of this five-year project include: (1) Large-scale EM analyses to characterize pieces of importance to the penetration and coupling of UWB and HPM sources into modern electronic circuits and systems. EM field solvers based on hybrid finite element/method of moment and Time-domain hybrid method are now become available for radiation and scattering of HPM or UWB pulses from large targets (aircraft, vehicles, boxes, etc.) with penetrating wires, apertures, cracks, doors, and antennas. **(2). Digital-circuit nonlinear transient simulators that go beyond the traditional SPICE model by including the full-wave**

electric-circuit model for passive linear components and transmission lines. Full three-dimensional EM field solvers for integrated circuits with implemented fast multi-pole reduced-order algorithm combined with nonlinear circuit model are available now commercially through this MURI project. We also delivered the EM solvers with the capability of converting the HPM/UWB signals into current sources of the linear and nonlinear circuit models of digital circuits for SPICE simulation. **(3). High-level understanding and description of the salient features of the spurious signals that alter the digital devices and computer systems operation states, based on nonlinear transient simulation of selected examples of nonlinear circuits.** Analysis from algorithm-based fault tolerance and central-flow oriented watchdog monitoring for program error determination and classification are now available for digital circuits and systems under EM threat. The analysis also includes the capability of determining the occurring frequency for various types of faults (data errors, control flow errors, program crashes, and a hung processor). **(4). Experimental and analytic validation of the EM solvers for canonical pieces; System-level measurements for overall coupling model validation; Experiments for validation and demonstration of high-power EMI effects at a component, circuit, and system level; Design and analysis of large overall digital systems. (5). A total number of 238 publications, of which 68 were technical reports or journal articles, an advanced graduate course on EMC/EMI for the internet, and a special issue on *Electromagnetics* was devoted to this MURI project. (6) Fortyseven students who received MS and PhD degrees worked on topics related to this MURI project. (7) We also collaborated with members of the other MURI teams at the University of Maryland.**

I. INTRODUCTION AND ACCOMPLISHED OBJECTIVES

Over the past 30 years, significant progress has been made in understanding and mitigating the effects of nuclear electromagnetic pulse (NEMP) fields on electrical systems. Starting from early documents on the characteristics of NEMP and running through recent IEC committee work on developing standards for NEMP protection, there are clear-cut guidelines on protection methods and designs for hardening such systems. NEMP protection guidelines have been incorporated into the construction of military facilities, and test facilities and procedures for the NEMP environments have been developed. Recently, other EM threats have been developed or postulated, including the ultra wide-band (UWB) environment and narrow band, high power microwave (HPM) sources with operating frequency spectra extending well beyond several GHz. Such signals are collectively denoted as "high power electromagnetic" (HPEM) environments. Coupled with the fact that modern electrical circuits and systems have become increasingly digital, it is evident that many of the HEMP test and analysis procedures developed for analog systems are no longer appropriate for digital equipment. Thus, we need to extend our present thinking of system-level interactions to include modern digital systems.

For modern digital systems subjected to HPEM excitation, the analysis and methodology need to be redeveloped and tested. Conventional radio frequency (RF) lumped-circuit concepts are no longer appropriate in microwave regimes. Simple traces become dispersive transmission lines and interconnects become passive distributed circuit components. Moreover, small elements of the system become comparable to a wavelength and are no longer negligible. Electromagnetic coupling between various components becomes much more important. Many of the standard approaches or common rules are no longer appropriate. In particular, the following issues need to be addressed:

• Modification of topological decomposition concepts to include high-frequency effects and distributed field excitations.
• Extension of the coupling, penetration and propagation models to the higher of HPEM stresses.
• Development of a better understanding of the behavior of digital components and systems subjected to EM stresses, including failure mechanisms of individual components and logic upset, latch-up or failure of systems of digital components.

A digital system can be in many different states, depending on its internal functioning, and its response to an external EM stimulus may depend on the "initial conditions" of the digital system. Moreover, in current HEMP testing, there is usually no control of the software features or changes made to the tested equipment, since only the hardware is considered of real importance. For a digital system, its operating software is often changed and modified for testing, so that the real properties of the system may not be present in the tested system. Thus, we must develop a suitable test protocol for digital systems with rules for acceptable software flexibility, without recurring engineering costs. This project investigated advanced modeling and analysis of digital systems subjected to an UWB or HPM environment to address these needs.

The overall objective of this research is to develop analysis and design tools with verification for electronic systems under HPM or UWB environments. Key to our technical approach is the concept of *electromagnetic topology*, which permits the subdivision of a complex EM system problem into smaller pieces that can be analyzed separately with high accuracy and efficiency. Each piece is treated as an N-port network and modeled by a generalized scattering matrix. The EM coupling of all pieces is modeled through the cascade of all scattering matrices. Based on this topology concept, our effort is focused on four interactive tasks.

Task 1. Numerically model penetration and coupling of HPM and UWB sources into large-scale, complex structures. This task developed EM models of field penetration due to HPM/UWB signals generated by some exterior or interior sources. The analysis involves features of the exterior and interior of the system as well as that of aperture(s) through which the signal penetrates the system. A system is divided into many sub-systems (pieces) and each can be analyzed thoroughly by a frequency-domain integral-equation moment method, a hybrid finite element method, or a time-domain integral-equation method. Example pieces are: 1) Black boxes with pins/connectors; 2) Cable bundles; 3) Cavities with apertures; 4) Cavities containing cable bundles; 5) Antennas as direct (front door) and out-of-band (back door) entry ports; 6) Aperture with cable bundle passing through; 7) Aperture in cavity with cable bundle passing through; 8) Seams in surfaces; 9) Protected buildings like a concrete block house with rebar and other metal constituents.

We have modeled the penetration into structures such as slots in a conducting plane backed by a channel and cascaded cylindrical cavities. Electromagnetic wave coupling to the interior of a cavity was successfully analyzed using a hybrid approach that maximizes the use of circuit theory and transmission line theory to reduce the computational effort. Our results were validated by comparison with exact full wave methods. The BLT equation is a frequency-domain matrix equation describing the behavior of the voltages and currents at all of the junctions (interconnections) of the multi-conductor cables in the network. We have extended the BLT formalism to include the distributed interaction between electromagnetic fields and the transmission line cables. We have provided a time-domain version of the BLT equation, which allows for the description of interaction with non-linear loads. We have included fields into the formalism of the BLT, which allows using a network formalism to study the penetration of fields through apertures. Finally, we have also developed a hybrid S-parameter characterization of

transmission line networks connected to non-linear loads. There are applications where the exact location of cables is not known. Hence, we developed a theory for random multi-conductor transmission lines, where the randomness is associated with the position of the cables, and we have derived expressions for the probability density function of the terminal voltages that appear to be in very good agreement with experimental results previously find by the Air Force Laboratory.

Task 2. Numerically analyze conducting and radiating EMI from HPM and UWB sources on printed circuit boards and integrated circuits. This task determines the spurious or modulating signal waveform at the chip or digital electronic circuits from the knowledge of the penetrated signals from HPM/UWB sources. In order to accomplish this goal, we have developed three major modeling and simulation capabilities. (1). A network oriented nonlinear transient simulator that goes beyond the traditional SPICE-based transient simulators. It accounts additionally for the distributed electromagnetic nature of the coupling paths (traces, passive components, etc.) yet accommodates fully small-signal and large-signal models for the nonlinear electronics. (2). Electrical circuit models for coupling paths to be used in the nonlinear transient simulator. (3). A rigorous and expedient electromagnetic modeling capability that converts the radiating and conducting EMI into a set of noise sources to be used in the nonlinear transient simulator. An important feature of our model development is that we separate the electromagnetic field analysis from the nonlinear circuit analysis, with the understanding that the dimensions of nonlinear components are much smaller than the smallest wavelength of EMI noise.

Our accomplishments include fast general purpose large scale solvers in both the frequency- and the time-domain. We have also produced hybrid solvers that combine the method of moments and SPICE to study transmission lines in the presence of complex structures.

Task 3. Analyze the excitation and response of digital circuits/systems to HPW/UWB signals. This task evaluated by analysis at the board and device level the effects of HPW/UWB sources on the digital device behavior. Chip or digital electronic circuit reactions to a given spurious waveform and the resulting alteration of the function and/or performance of the digital logic will be investigated. There are two main objectives in this task. (1) to understand and describe the salient features of the types of spurious signals that can cause a change in state in a representative set of digital logic circuits or systems. (2) to describe what an unintentional change in state, or changes in state at several locations, will do to the function and/or output of a digital system. The SPICE model and the nonlinear transient circuit simulators in **Task 2** were used to achieve the objectives.

The interference was modelled as a noise in the form of a single-frequency sinusoid or a pulse train and is superposed to the pulse trains of the digital signals. SPICE simulations for examples of digital circuits were performed to determine the threshold of the state change (error bits) under various interference frequencies and voltage levels. Propagation effect of error bits through the circuits was also investigated. Bit error rates at the input and output pins are further related to the external microwave source for the case of a wire penetrating a cavity aperture.

Task 4. Develop and implement methods for validating HPM/UWB coupling models / Design large and small scale (subsystem) experiments. Models of EM interaction with systems and components, and their numerical realizations (codes), are only approximations to the real world. They can be easily used to perform sensitivity studies, to evaluate hardening concepts and to design new, well-protected systems. However, such computational models must be validated, and the best way of doing this is to perform simulation and measurements on selected systems

and components, or on suitable canonical representations of the same. In addition, it is necessary that those who work with EM interaction with systems understand the fundamental mechanisms involved in coupling. They should strive to develop the experience needed to identify in a system of interest the presence or not of the major mechanisms or physical structures which are known to influence coupling from point-to-point within the physical volume of the system.

The objective of this task is three-fold: (1) to develop and implement the methods for validating the EM coupling, penetration, and propagation models; (2) to develop, standardize and use test concepts suitable for understanding how high-power electromagnetic (HPEM)-induced stresses at the component (chip) level affect the operation of the circuitry; and, (3) to develop and describe simple experiments whose performance and study will enable a user to understand the major mechanisms that influence the changes experienced by a signal as it makes its way from one point to another in a system.

The investigations were will be both numerical and experimental to enable the user to validate the accuracy of numerical data obtained for a selected subset of the *pieces* described elsewhere in this proposal. Additionally, they enable the user to appreciate and validate the topological notions that are at the basis of the approach taken in this MURI.

Our accomplishments include the production of several exact solutions for the radiation, penetration, and scattering from bodies of simple shapes for which an exact analytical solution is possible. These exact solutions find application in the validation of the numerical solutions obtained with numerical solvers for EM problems.

II. RESEARCH CONTRIBUTIONS

2.1) UNIVERSITY OF ILLINOIS AT CHICAGO

New canonical problems

Exact analytical solutions to boundary-value problems for complicated structures containing a cavity, sharp metallic edges, and different penetrable media were presented. The geometries include metallic cavities of semielliptical or semispheroidal cross-section flush-mounted under a metallic infinite plane. The cavities are filled with isorefractive materials. The solutions are found for primary fields that include dipole sources, plane waves or line sources. A list of the geometries is shown in Fig. 1. The solutions are determined by expanding the primary and secondary fields in infinite series of eigenfunctions involving the products of radial and angular Mathieu functions or spheroidal functions and by imposing the boundary and radiation conditions. This process leads to the analytical determination of all modal coefficients in the eigenfunction expansions. Thus, the obtained solutions are exact and constitute new canonical solutions of boundary-value problems. The exact analytical solutions for the new canonical problems allow us to validate and check the large-scale EM solvers we developed to analyze pieces. Measurements were also made to validate the analytical solutions for the new canonical problems and to validate the hybrid method for the coupling into cavities.

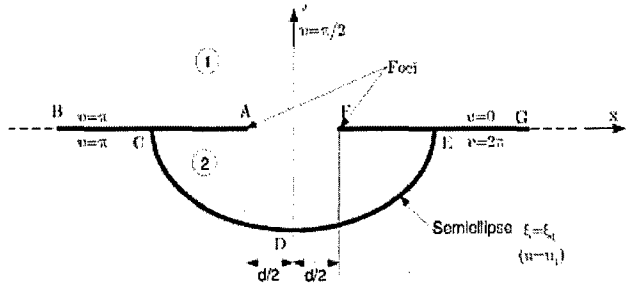

(a). Semi-elliptical-Channel-Backed Slotted Screen

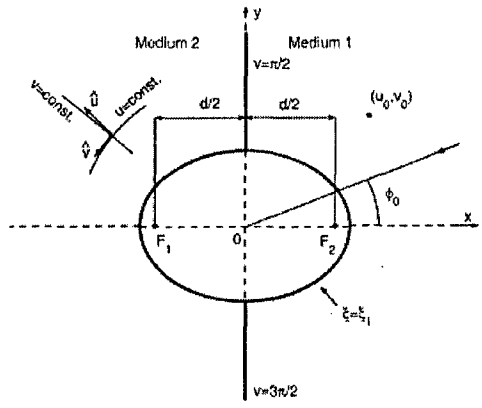

(b). An Elliptic Metal Cylinder at the Interface between Isorefractive Half-spaces

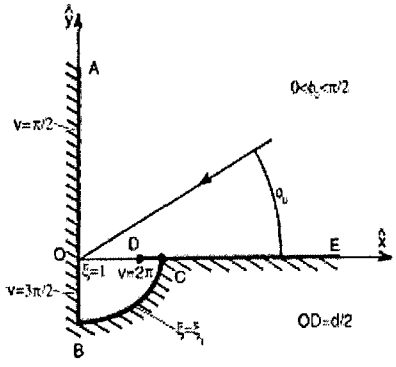

(c). Cavity-Backed Gap in a Corner

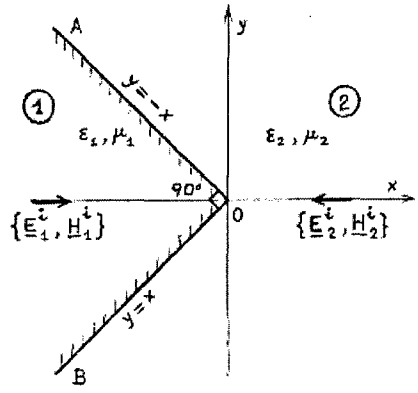

(d). A Right-Angle Isorefractive Wedge Structure

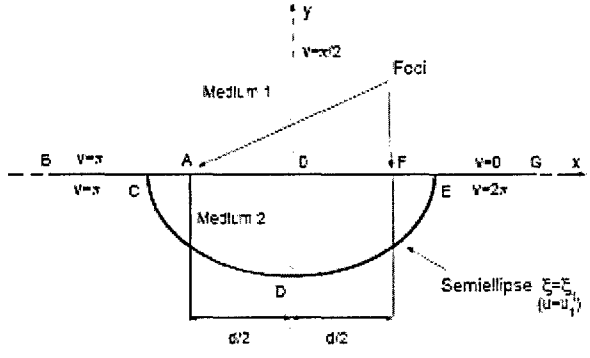

(e). A Slotted Semi-elliptical Channel Filled with Isorefractive Material

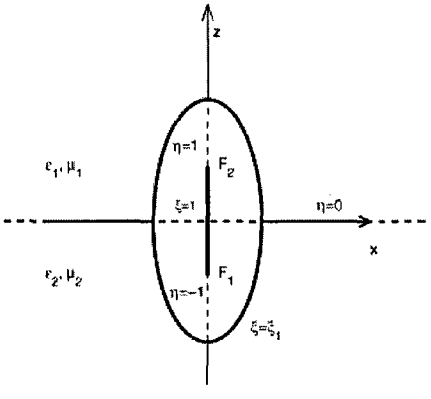

(f). Metallic Spheroids at the Interface Between Isorefractive Half-Spaces

Fig. 1. A list of canonical geometries that are solved analytically for the validation of large-scale EM solvers developed in this project.

Analysis of RF Radiation Interference on Wireless Communication Systems

Advanced wireless communications including both RF analog and digital circuits have the features of small size, low power, low cost, and transmitting high date-rate signals. Signal interference with external power sources enter mostly through the front-end antenna and the effect appears on the BER of the base-band digital signals. We combined EM and communication theory to investigate the radiation noise effects. First, EM simulation is performed to determine the radiation noise power at the chip input pin due to the external power source. Communication theory taking into account the fast fading due to random multipath signals is used to relate the BER to SNR of the systems. This method applies primarily to the low-power case, where the front-end LNA is still operated in the linear region with the presence of radiation noise. The proposed method provides a statistic and much simplified system approach to evaluate the effects of radiation interference to a communication system.

An example of a complete communication system for a wireless mouth is shown in Fig. 2. It was built on a 1 by 3 cm FR4 printed circuit board (PCB). A chip antenna is placed on the left-front corner and a 7mm by 6mm chip with both RF and digital systems is packaged in the middle of the board. The PCB is placed inside a PC mouth for wireless communication at the frequency band of 2.4-2.47 GHz. The small board tuning passives are neglected in EM analysis. The grounded FR4 PCB board is 40- mil thick and has a dielectric constant of 4.2. A bended inverted F antenna is connected to the communication chip through a 50 Ohm metal trace. Note that the metal ground is removed underneath the F antenna. The whole structure is simulated with Ansoft HFSS software. Metal trace to the chip input pin is assumed terminated with a 50 ohm load. Full-wave simulation is to determine the induced electric field (or induced voltage) at the chip input pin, where the input impedance to the entire electronic system inside the chip is assumed tuned to a 50 Ohm load. The incident field is assumed polarized in the plane of the PCB board ($\theta = 90$ degrees) (vertical polarization to the plane has little effect to the PCB Board) with strength 1V/m and $f = 2.44$ GHz. This field corresponds to a microwave source 12.2dBm transmitted power at 1meter away with 0dB directivity. Induced power at the chip pin input versus the ϕ angle from simulation is shown in Figure 3. This input power is considered the noise input to the system. This radiation noise adds to the system noise reducing the overall system SNR and the bit error rate (BER) of the base-band digital signals.

For binary phase shift keying (BPSK) in the additive white Gaussian noise (AWGN) channel, the BER is given as

$$\text{BER} = \frac{1}{\sqrt{\pi}} \int_{\sqrt{\gamma}}^{\infty} e^{-x^2} dx \text{ , where } \gamma \text{ is the signal to noise ratio.} \qquad (1)$$

AWGN channel is for the line of sight (LOS) signal path and is a reasonable assumption here for a wireless mouth dongle. When the received signal is composed of the LOS signal and a random multi-path component, the BER would be based on a Rice channel model.

For a good design, the system noise N_s in a small communication system is less -90dBm and the sensitivity of the receiving system is defined as the minimum received noiseless signal energy such that BER is less than 0.1%. If we ignore the system noise (several order of magnitude less than the radiation noise), SNR in dB can be written as

$$\text{SNR} \approx S - N_m(\phi) + 12.2 - x \text{ ,} \qquad (2)$$

where S is the signal, $N_m(\phi)$ is the radiation noise induced at the input pin given in Figure 3, and x is the microwave source power (dBm) 1 meter away from the system. Radiation interference of the communication system is characterized by the BER at base-band versus the external noise source power for a given received signal. As an example, assuming that the signal power is -50 dBm, Figure 4 shows the BER as a function of the external microwave power. Note that if we fix $N_m(\phi)$, increasing the distance by a factor of two corresponds to increasing the noise power source by 6dB. Figure 4 also shows that the noise power due to the incident field from either the left or right side of the dongle is much stronger than from the front, a result of the front-end linear antenna orientation. For a -50 dBm signal, a 20 dBm external source 10 meter away will result in the worst case of about 15% BER, far beyond what a system can tolerate.

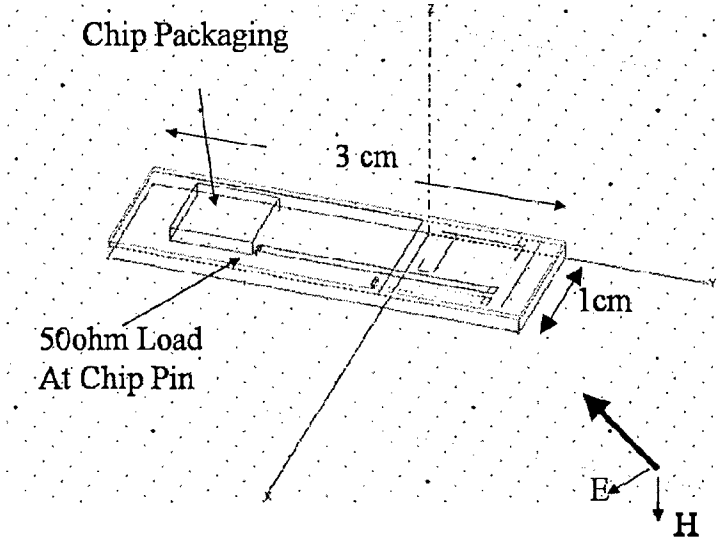

Figure 2. External microwave source interaction with a dongle for a wireless mouth. Incident field is polarized in the x-y plane ($\theta = 90^o$).

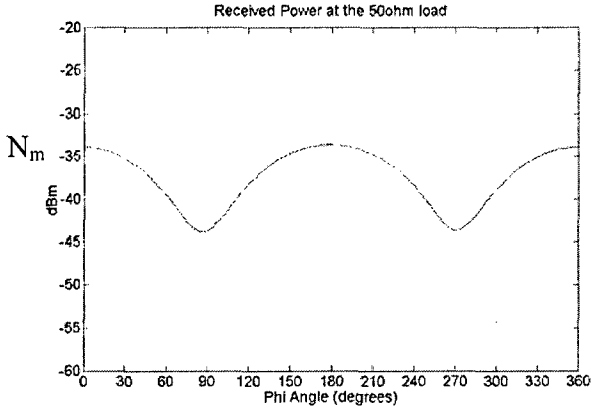

Fig. 3. Induced radiation noise at the input pin of a dongle obtained by HFSS simulation. 0 dB directivity microwave source transmits 12.2 dBm power at 1 meter away at $f = 2.44$ GHz.

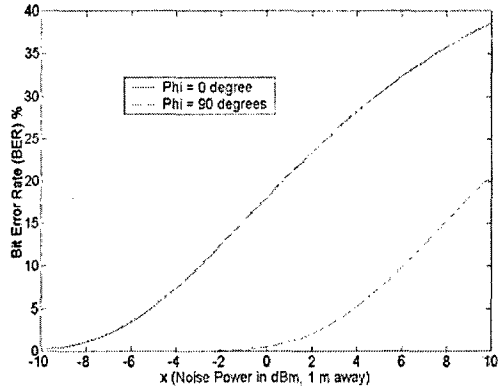

Figure 4. Bit error rate of the dongle as a function of external microwave source for $f = 2.44$ GHz and signal power -50 dBm.

Analysis of High-Power RF Interference on Digital Circuits

In the analysis of intentional high-power RF interference on digital circuits, the interference is modelled as a noise in the form of a single-frequency pulse train (sinusoids or square waves) and is superposed to the pulse trains of the digital signals. SPICE simulations for a CMOS inverter and a 4-bit adder are performed to determine error bits at the circuit output with EMI injected at the input port for various interference frequencies and voltage levels. Propagation effect of error bits through the circuits is investigated. It is found that in general the digital circuits will reduce the error bit rates as signals propagate through when the EMI frequency is much higher than the signal frequency. Error bit rate amplifies when the EMI frequency is close to the signal frequency. The phase difference between EMI noise and signal also affects the bit errors. Bit error rate is further related to the external microwave source for the case of a wire penetrating a cavity aperture.

For high-power interference, we investigate the digital bit error due to EMI sinusoids at various voltage levels comparable to the transistor bias voltage. Common EMI voltage amplitude and frequency due to the circuit cross talk and coupling are much smaller. The EMI of interest here are those due to external high-power microwave sources. It is of interest to know how the high-power microwave sources are related to the EMI voltage. This analysis usually requires EM simulation of the EM field penetrating through the system into the circuit pins. An example for a field wire penetrating an aperture in a conducting cavity and in contact with a transmission-line wire is used here for demonstration. The physical geometry is shown in Fig. 5. The EMI voltage levels at the pins of interest here are in the range of 1 to 4V. Assuming that the high-power microwave sources radiate uniformly, it is found from the work of University of Houston (to be addressed later) that 1V 0.5GHz EMI at the transistor pin corresponding to 38.2dBm transmitted power 1m away from the box. If the source moves farther away from the box, the required power level increases in order to induce same amount of voltage at circuit pins.

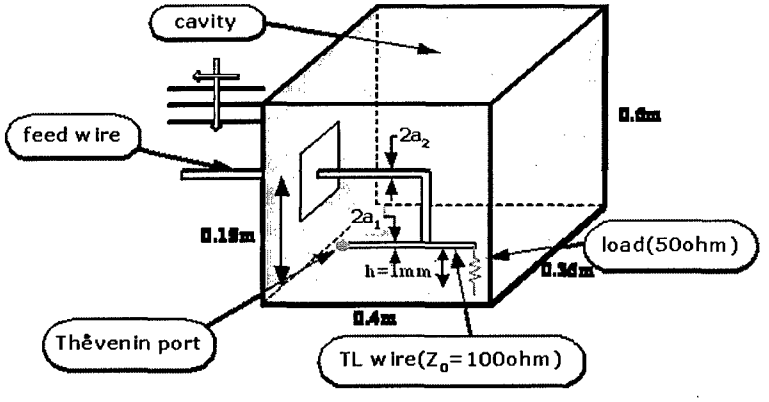

Figure 5. A feed wire penetrating an aperture in a conducting cavity and in contact with a transmission-line wire.

The formula for 0.5GHz transmitted power from the source is given as

$$P_t = 20\log_{10}(V_{inc}) + 20\log_{10}(r) - D + 38.2 \ \text{(dBm)} \ , \qquad (3)$$

where V_{inc} (in volts) is the induced voltage at the circuit pin, r (meters) is the distance of the

source to the box aperture, and D is the directivity of the high-power source. Similar formula can be derived for various EMI frequencies. (3) is useful to determine the required transmitted power to achieve a specific bit error rate at the output of a digital circuit. In this paper, V_{inc} and EMI frequency is assumed at the input port and we investigate its effect to the digital bit errors.

As an example, the investigation of EMI on digital systems is for the case of a 4-bit adder shown in Figure 6. There are a total of 4 sub-circuits, each consisting of 28 CMOS transistors. In each sub-circuit, there are three inputs (two bytes for addition and one from carry over) and two outputs (one is the sum and another is the carry-over).

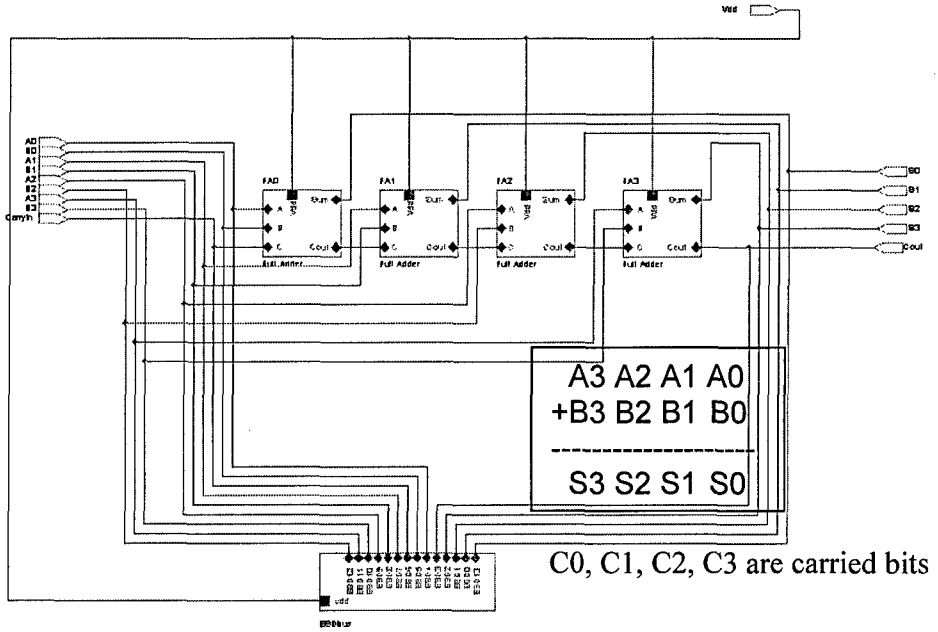

Fig. 6. The circuit diagram of a 4-bit adder.

The transistors are assumed based on a 0.18um BSIM3.1 (Berkeley Short-Channel IGFET model) process. The channel width for PMOS is 0.81um and for NMOS is 0.27um. The circuit parameters are found through MOSIS for SPICE simulation. In the 4-bit adder, each bit is either 1 or 0 and the input bits are A3 A2 A1 A0 (as one number) and B3 B2 B1 B0 (as another number). The output bits are S3 S2 S1 S0 (as one number) with C3, C2, C1, and C0 as the carried bits in the adder. Strictly speaking, C3 is also the first bit of the 5bit output. As an example, in the EMI analysis, the EMI waveform is injected at the B0 pin with B1, B2, and B3 are all assumed 0. The digital pulse trains are set for A3, A2, A1, and A0 with the corresponding output pulse trains (S3, S2, S1, and S0). The scheme to investigate the EMI effects on this full 4bit adder is to inject EMI at B0 pin and the bit error rate (BER) for B0 is evaluated. The BER at the output pins S0, S1, S2, and S3 are also evaluated with EMI presented at B0 pin. The comparison of BER at the input and output pins demonstrates the EMI effect through the adder.

Due to the simplicity of the circuit, for the inverter, we focus on the EMI voltage level below the threshold voltage (2.5V) to investigate the modulated effect of the EMI sinusoid. For a 4-bit adder, on the other hand, due to the circuit complexity, we investigate mostly the case where EMI voltage level is above the threshold voltage and the overall EMI effect is more noticeable.

EMI voltage level versus BER at input and output pins is shown in Fig. 7 for 0.5GHz EMI. First of all, when the EMI voltage level is across the threshold voltage (2.5V), BER at input and

output pins increases dramatically, where the EMI voltage is sufficient large to cause error bits even outside the transient zone (rise and fall time). For a smaller EMI voltage, where its effect is mostly in the transient region, it is seen that voltage level is insignificant to the BER. It is also observed that the BER at S0, the direct output from the input pin B0, is much higher than the rest pins. The error bits at B0 propagate to S1, S2, and S3 pins through the carried bits C0, C1, and C2. It is seen that errors at the carried bits reduce as the signals pass from one adder sub-circuit to the next. Overall, the output BER is less than the input BER in the over-threshold region. This implies that when there is large voltage swing in the input pin, the system has little time to react the sudden large change in voltage. As a result, the output errors are less. This observation is further illustrated through the example in Figure 81, where the case is similar to that in Figure 7 except the EMI voltage frequency is 1GHz. Comparing the two cases (1GHz and 0.5GHZ EMI), one sees that for higher EMI frequencies, the BER is much less in the output pins (10% or so). Investigating the BER for many EMI frequencies, one observes that the BER is consistently lower at higher EMI frequencies. The investigation here provides a preliminary study of the effects of high-voltage (comparable to threshold voltage) and high frequency (in GHz range) EMI on high-speed digital circuits.

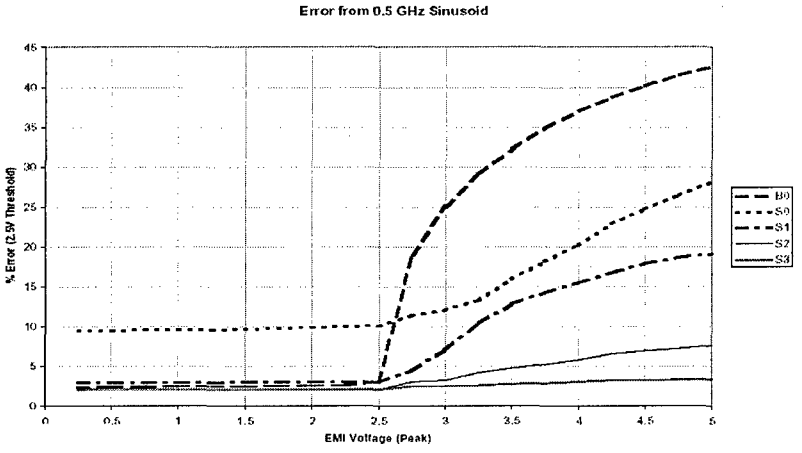

Fig. 7. Bit error rate at the 4-bit adder I/O versus EMI voltage for 0.5GHz pulse train interference at the input B0 pin. Input is 5V 100 MHz pulse trains.

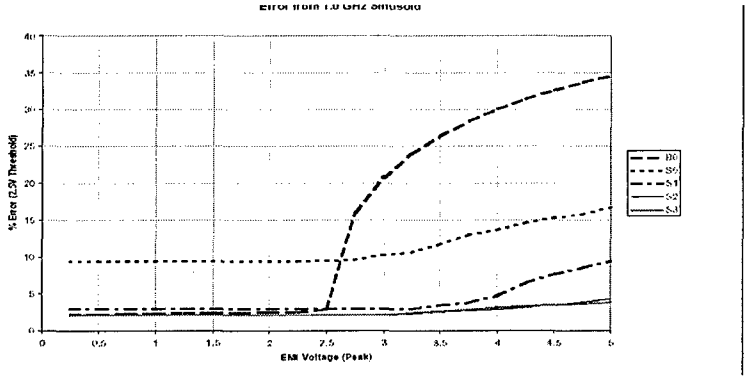

Fig. 8. Bit error rate at the 4-bit adder I/O versus EMI voltage for 1GHz pulse train interference at the input B0 pin. Input is 5V 100 MHz pulse trains.

Off-Chip Control Flow Checking of On-Chip Processor-Cache Instruction Stream

We have developed novel techniques for off-chip CFC of a processor with on-chip caches - the first time such techniques have been developed to the best of our knowledge. Our techniques involve sending a subset of instructions in a block from the CPU to the off-chip watchdog processor (WP) - the subset size depends on the bandwidth mismatch K between the CPU-cache bus and the system bus, the concept of K alternate derived-signatures per block, and the concept of NOP insertion for relative primality of K with respect to loop sizes - this facilitates checking of almost all instructions of each loop over multiple loop iterations. The results show effective block-level error coverage (BEC) of 80-93% for high fault frequencies and of 70-94% for low fault frequencies, and almost 100% program level error coverage (meaning that error(s) in the program execution are detected at some point in the program execution, even if each erroneous block is not detected during the block's execution), which facilitates reliable fail-safe operation. These results underscore the overall efficacy of our techniques, and thus makes it viable for commodity processor systems (with minor overheads for enabling off-chip CFC) to be plugged in with an external WP when concurrent error checking is desired.

2.2) CLEMSON UNIVERSITY

Classification of EMI effects

One can classify potential intentional electromagnetic environments (IEME) threat environments into four categories, based on the frequency content of their spectral densities as "narrowband," "moderate band," "ultra-moderate band" and "hyper-band."

Another approach for characterizing the IEME produced by a HPEM source is to examine the E-field strength at a specified distance from the source, the frequency agility of the source, the duration and repetition rates for pulsed sources, and the burst lengths. For IEME frequencies in the range of 200 MHz to 5 GHz (λ varying from 150 to 6 cm) the feed and antenna structures for the radiating systems typically consist of electromagnetic horns and reflectors, so aperture antenna theory provides some information about the radiated EM field behavior. Typical CW source powers from readily available sources can range from 1 kW (for a simple microwave oven source) to over 10 MW (for radar tubes). From readily available microwave sources, it is possible to produce on-target E-fields greater than 100 V/m at kilometer distances. Considering the possible effect of these fields on illuminated equipment, the L band frequency range is likely to cause more electronic damage than at the higher frequency bands (i.e., 10-GHz radar).

Another way of categorizing IEME environments is based on the level of sophistication of the underlying technologies involved in producing the EM environment, as low, medium, and high-tech systems. The low-tech systems are characterized by: 1) marginal performance; 2) minimal technical capabilities; and 3) easily assembled and deployed while hiding behind dielectric walls in trucks and similar vehicles. In contrast, medium-tech systems require the skills of a qualified electrical engineer and relatively more sophisticated components such as a commercially available radar system that can be modified to become a weapon system. More sophisticated high-tech and high-power electromagnetic (HPEM) systems would require specialized and sophisticated technologies and perhaps even specifically tuned to cause severe damage to a specific target.

A. Low-Tech Generator Systems. Due to its simplicity, a readily available low-tech CW microwave source in the S band (2.45 GHz) is the magnetron in a microwave oven. Typical and

readily available microwave ovens are rated at 800 to 1500Wof rms continuous microwave power. With 1100W of rms continuous microwave power at 2.45 GHz from a microwave oven, the peak electric field in the output waveguide is about 25 kV/m. This low-tech system was used in exposing several test objects such as calculators, wrist watches, electro-explosive devices, florescent tubes, etc., with significant adverse effects (upset and burn out) .

B. Medium-Tech Generator Systems. Commercially available radars can be modified to become an HPEM system (narrowband or ultra wideband, and this is an example of a medium-tech system. Examples of complete systems offered for sale by Radio Research Instruments Co., Inc., Waterbury, CT, are the AN/FPS-36, AN/FPS-71, AN/FPS-7, and AN/FPS-77. This commercially available system is powered by a 5-MW magnetron source.

C. High-Tech Generator Systems. The high-tech systems require specialized and sophisticated technologies in their construction. Examples of such IEME generators are the IRAs. An IRA with a diameter of 23 cm is shown in Fig. 9. This antenna has been excited with a commercially available pulsed voltage source (pulser) having a peak voltage amplitude of 2.5 kV, a rise time of 100 ps, full-width to half-maximum (FWHM) pulse width of 2 ns, and a of 500 Hz. The above IRA is one of many that have been fabricated and tested. All of the high-technology systems are hyper-band HPEM generators, since their band ratios are 10. However, it is observed that they can also be turned into sub-hyper band generators by reducing the antenna diameter (which is seen to increase the lower cutoff frequency of the system) or by degrading the rise time of the voltage pulse into the antenna (which can be shown to lower the upper cutoff frequency of the radiated spectrum).

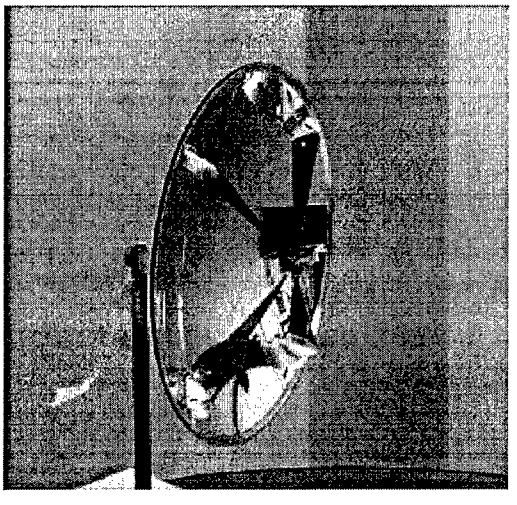

Fig. 9. IRA with a diameter of 23 cm; a component of a high-tech IEMI system.

Extension of the BLT equation

The usual Baum-Liu-Tesche (BLT) equation describes the propagation of voltage (and current) waves along transmission lines. The BLT equation was extended from the frequency domain into the time domain to permit an analysis of a transmission line with nonlinear loads at each end of the line. The BLT equation was also extended to include the effects of propagating EM fields and their coupling to transmission line structures. In the extended BLT formalism,

both voltage and E-field quantities are treated together and this permits the addition of scatterers and apertures in the models.

The problem to be discussed here is shown in Fig. 10. It consists of a lossy transmission line of length L, with time dependent and/or nonlinear loads $Z_{L1}(t)$ and $Z_{L2}(t)$ at each end of the line. The line is excited by a lumped transient voltage and current source at location $x = xs$. For this problem the transient load voltages and currents at each end ($v1(t)$, $i1(t)$) and ($v2(t)$, $i2(t)$) are required.

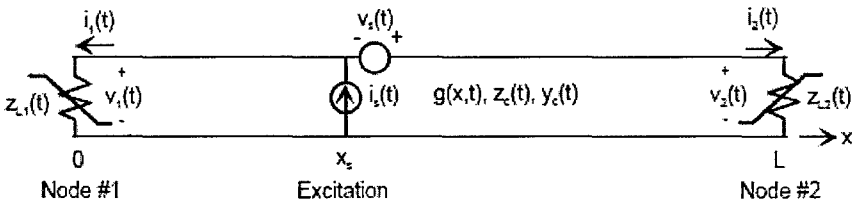

Fig. 10. A lossy transmission line with nonlinear loads at each end and excited by lumped transient voltage and current sources.

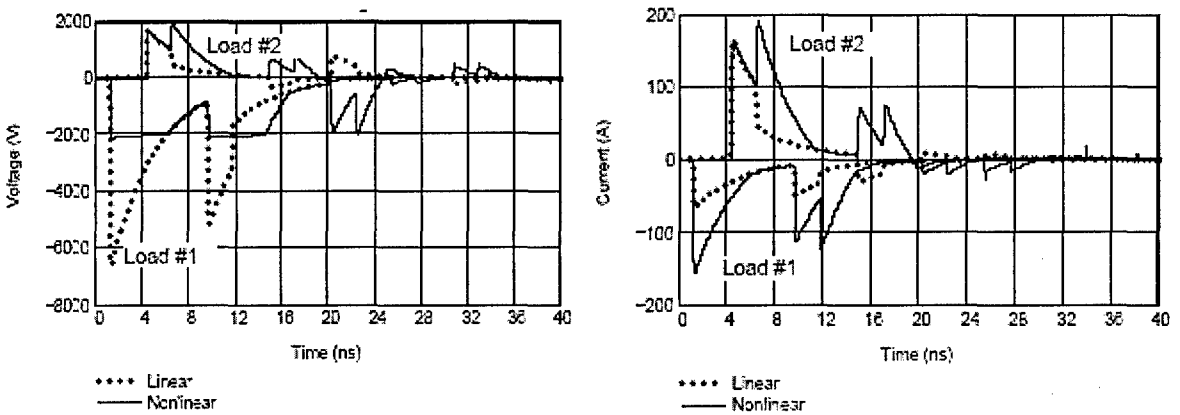

a. Load Voltages b. Load Currents

Fig. 11. Plots of the load voltages and currents for the case of the line with a nonlinear resistance at load #1. (Solid lines are for the nonlinear response, and the dotted lines represent the linear solution.)

The solid curves in Fig. 11 represent the transient load voltages and currents for the nonlinear element located at load #1. Shown by the dotted lines are the corresponding linear load responses. We note in Fig. 11 that the load #1 voltage is clipped at about -2 kV, and that as a consequence, the current flowing through this load is about a factor of 2 larger than that for the linear load. It is also apparent from Fig. 11 that the operation of the nonlinear element at load #1 affects the response at load #2. For the nonlinear element present, we note that there is an increase in the amplitudes of both the voltage and current across $RL2$ and the pulse duration is longer. Thus, there is more instantaneous power delivered to $RL2$, with an increased chance of failure in this element. This example illustrates the well-known effect of a protective device (a voltage clamp in this case) increasing the stress on other components in the system. It is necessary to use the transient BLT equations for both the load voltages and the load currents, and

relate these to each other through the nonlinear v-i relationships of the terminations. This results in a nonlinear BLT matrix equation that must be stepped along in time to affect a solution. Several numerical examples have been presented in this paper to illustrate the use of this technique, and the results appear reasonable. While it is clear that this technique works well for simple resistive nonlinearities on a single transmission line, additional work needs to be undertaken in this area. Interesting issues for further study include:

- develop an extension of the present technique for nonlinear load analysis to a multi-conductor line and to a network of such lines,
- extend the BLT analysis to include energy storage elements, both linear and nonlinear, first for a single transmission line and later, for a network,
- develop the nonlinear BLT analysis for a distributed EM field excitation,
- investigate the effects of having dielectric loss in the cables, which provide an additional per-unit-length conductance in the solution, and
- extend the BLT solution to transmission systems (such as a strip-line) that are not strictly described by the *f* functional dependence of the line loss.

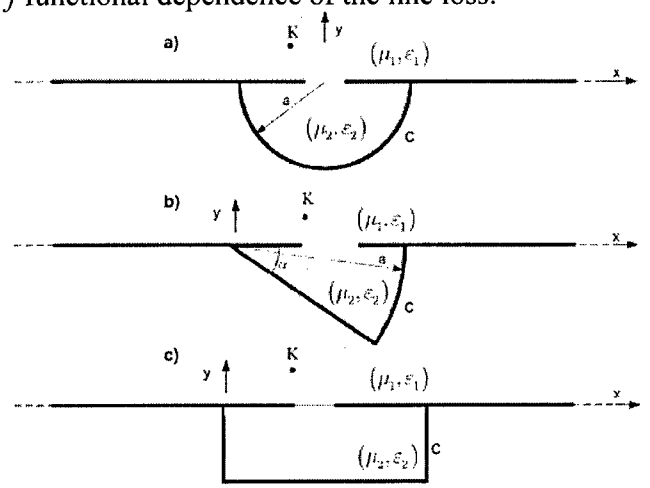

Fig. 12. Examples of channel-backed slots; a) hemi-cylinder-backed slot; b) Sector-backed slot; c) Rectangular-backed slot

Integral equation formulation for the penetration into cavities through apertures and its validation

Two types of integral equations are derived and solved for the unknowns associated with penetration of a field through a slot in a conducting plane backed by a channel. In one case the solution of a single integral equation allows one to determine all quantities of interest, while in the other coupled integral equations are solved for two unknowns knowledge of which enable one to characterize all quantities of interest. The coupled integral equation method is more general in that the configuration of the channel backing can be of arbitrary shape, but the other is more efficient since only one equation is involved. The boundary condition on the backing is enforced directly by one of the equations in the coupled equation method, while, in the single equation method, this condition is enforced by the inclusion of a backing-geometry-specific Green's function. Validations by comparisons with various analytical solutions developed at UIC were made. Examples of channel-backed slots investigated are shown in Fig. 12, including hemi-cylinder-backed slot, sector-backed slot, and rectangular-backed slot. The results of the comparison between the coupled integral equation method and the summation of analytic

formula of Mathieu functions are shown in Figs. 13 and 14, respectively for the H field and current density.

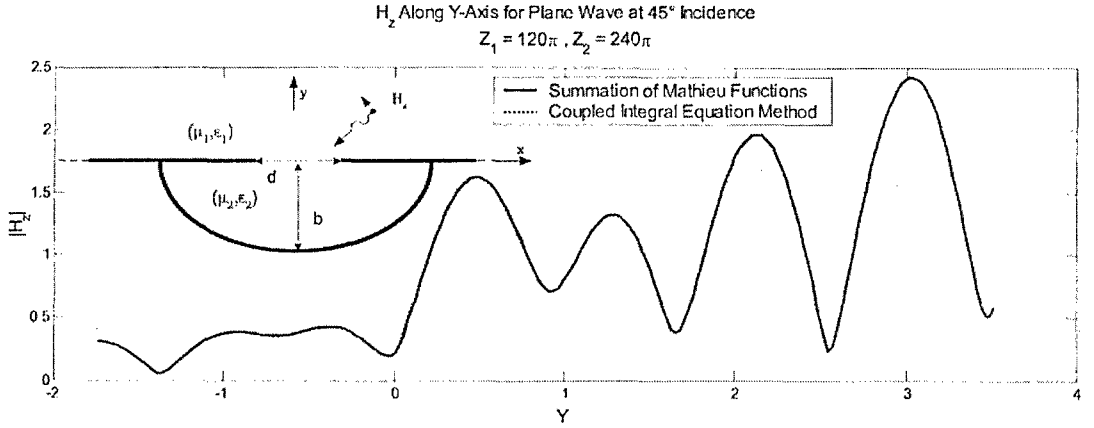

Fig. 13. Magnetic field along Y-axis for semi-elliptical-backed slot excited by plane wave of unity strength and incidence $\theta = 45^{O}$; $(\mu_1,\varepsilon_1) = (\mu_O,\varepsilon_O),(\mu_2,\varepsilon_2) = (2\mu_O,0.5\varepsilon_O)$; $d = 2$; $b = 1.732$; $f = 214.7$ MHz.

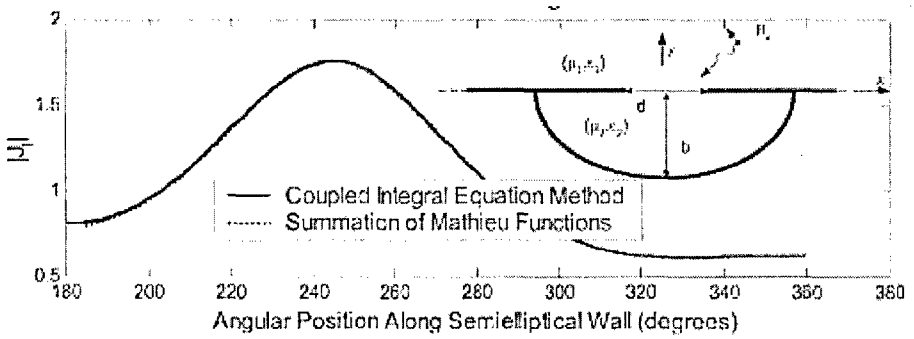

Fig. 14. Current density along Y-axis for semi-elliptical-backed slot excited by plane wave of unity strength and incidence $\theta = 45^{O}$; $(\mu_1,\varepsilon_1) = (\mu_O,\varepsilon_O),(\mu_2,\varepsilon_2) = (2\mu_O,0.5\varepsilon_O)$; $d = 2$; $b = 1.732$; $f = 214.7$ MHz.

Studies of propagation through cascaded structures

Theoretical and experimental studies of signal propagation through series of cascaded cavities connected by walls containing narrow slots and with thin wire probes/posts inside the cavities were developed. Coupled integral equations were formulated in terms of the electric current on the probes and the equivalent magnetic current in the slots and numerical solution techniques based on the moment method were used to solve them.

An example of the cascaded cavities is shown in Fig. 15. The cavities and baffles used for measurements are shown in Fig. 16. The geometry is a series of cascaded, axis-symmetric cylindrical cavities excited by a φ-independent source. The constituent cavities are either coaxial or circular-cylindrical. The field in each cavity is expressed in terms of the electric field in the apertures at the interfaces where adjacent cavities join. From knowledge of the aperture

fields, the complete field in the cavity structure can be determined. The frequency-domain data are used to compute the time-domain field in the system of cavities. Cavities were constructed and experiments performed to corroborate the computed data.

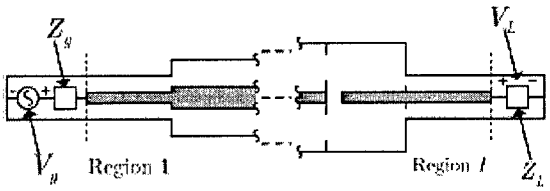

Fig. 15. Cascaded cavities.

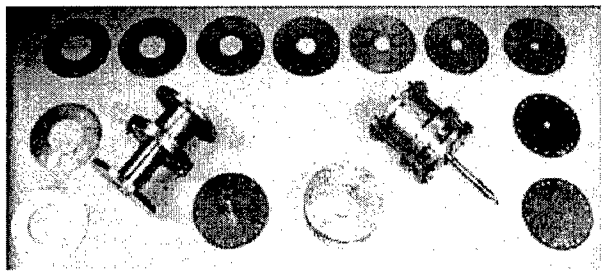

Fig. 16. Cavities and baffles used for measurements.

The cavity whose details are shown in Fig. 15 comprises three sections with dimensions and is terminated in a short. Good agreement is obtained in the measured and computed input admittances. The conductance displayed in Fig. 17 for the three-section cavity does not agree near resonances due to the large wall currents and the finite conductivity of the walls. When the cavity is terminated in an appreciable resistance, the load resistance prevents large wall currents, and the wall losses will be negligible.

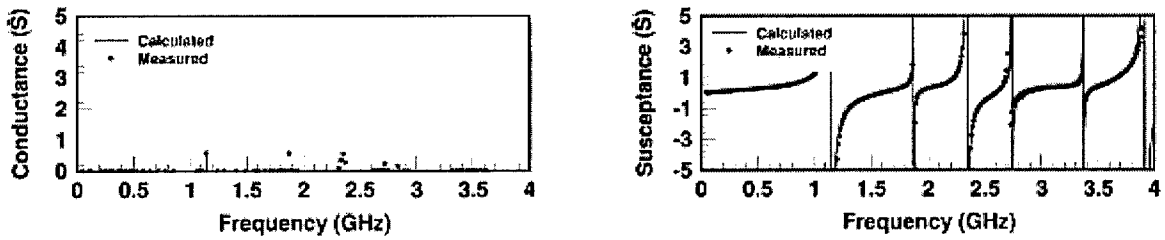

Fig. 17. Normalized input admittance of a three-section cavity terminated in a short (*a,* 0.7225, 10.21; *a,* 6.475, 5.13; 0, 6.475, 10.21).

The numerical technique is further extended to the constituent axisymmetric cavities with a cross-section that varies with axial displacement. A set of coupled integral equations are solved for the unknown electric fields in the apertures that separate the constituent cavities. Separate integral equations are formulated to determine the field in each cavity with a variable cross-section.

Several different axisymmetric pieces with non-uniform cross sections were machined for use as an inner conductor in the center cavity. For the first two models, the inner conductor pieces were constructed from two cylinders (S1 and S2), two conical pieces (S3 and S4), and two connectors (S5 and S6), which could be joined in any arbitrary order. These parts as well as their dimensions are shown in Fig. 18. The arrangement of the inner conductor parts in the center section is given from left to right in the format S5-S4LS2-S3R-S1-S6, where the L or R on S3 and S4 indicates that the large end of the conical section is situated on the left or on the right,

respectively. For model 1, the agreement between measured and computed data, shown in Fig. 19, is good at most frequencies but does exhibit some differences near 1 GHz and 2 GHz for a 50 Ω load. The two computational solutions agree very well.

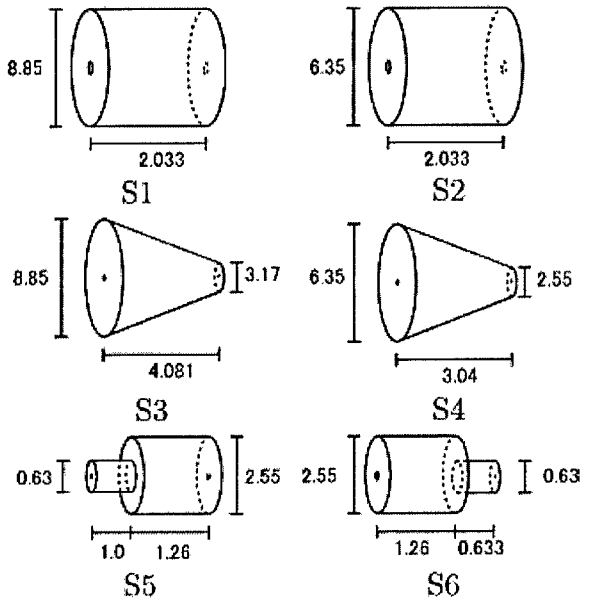

Fig. 18. Parts comprising variable cross-section center conductor (all dimensions in cm).

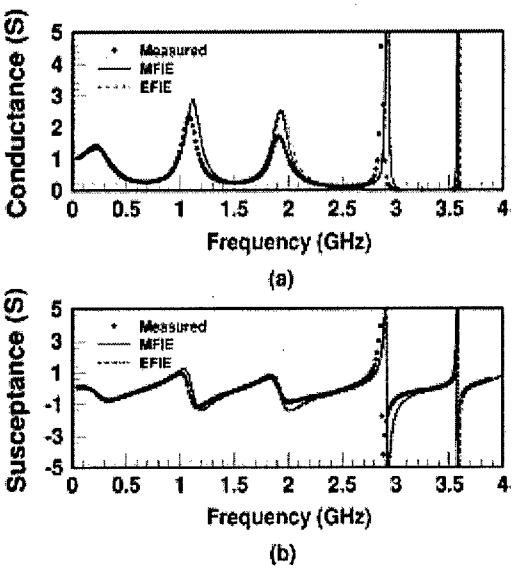

Fig. 19. Normalized input admittance for model 1 terminated in a 50 Ω load (S5-S4L-S2-S3R-S1-S6, $l3$ = 10.21 cm).

2.3) HOUSTON UNIVERSITY

Houston University concentrated its efforts on the development of an efficient hybrid method for calculating the EMC coupling to a device on a printed circuit board inside a cavity by a wire penetrating an aperture. This method assumes that the printed circuit board is connected to a wire or cable that penetrates through an aperture in the cavity enclosure. The method uses a combination of transmission-line analysis and a full-wave solver together with a decomposition of the problem into interior and exterior problems for maximum efficiency. The hybrid method was also extended to consider a time-domain excitation. The signal level at the input port of the device is calculated and studied. The incident electromagnetic field is assumed to be a time-domain plane wave in the form of a pulse, and two pulse shapes (a Gaussian pulse and an exponentially damped sinusoidal pulse) were studied. Results show how different pulse characteristics produce different types of signals at the input to the device. The time-domain results were validated by comparing with simple expressions based on the resonant frequencies and Q of the cavity.

1) Frequency-Domain Results. The sample problem selected for the results is shown in Fig. 20. A feed wire runs through a rectangular aperture on the side of a rectangular perfectly conducting cavity, and penetrates the cavity a distance of 20 cm before bending downward a distance of 14.9 cm to make contact with a transmission-line wire parallel to the bottom of the cavity. The radius of the feed wire is 0.25 mm, and it extends outside the cavity by a length of 12 cm. The feed wire is centered horizontally within the cavity along the dimension perpendicular to the transmission-line wire. For simplicity, there is no dielectric substrate, so the "substrate" is

simply a spacing of height h between the transmission-line wire and the bottom of the cavity. The transmission-line wire, which models a length of PCB trace, is chosen as a round wire for modeling simplicity. The wire has a radius chosen to give a 100 Ω characteristic impedance for this line. (The radius of the PCB line therefore changes as h changes. For example, for a substrate height of h = 1 mm, the PCB wire has a radius of 0.3833 mm.) Unless otherwise noted in the results, h is set to 1 mm. A 50 Ω load is connected at one end of the TX line. The transmission-line wire has length 26 cm, and the Thévenin port (the left end of the line) is located 10 cm from the closest perpendicular cavity wall. All other dimensions are given in Fig. 20.

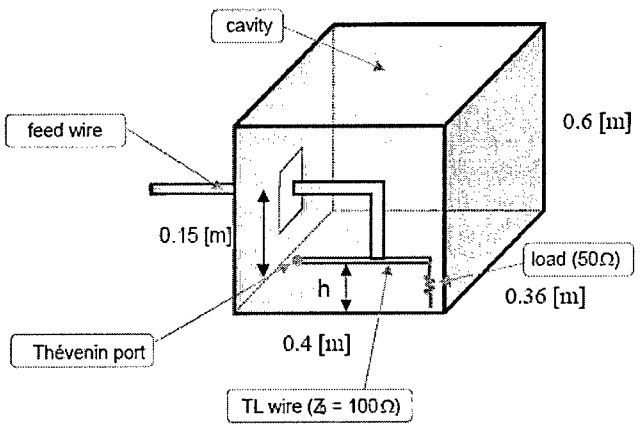

Fig. 20. Sample geometry used for the numerical results.

In the hybrid method, the PCB transmission line is modeled as a frequency dependent lumped load by using transmission line theory. The accuracy of the transmission-line theory depends on several factors. One of the dominant factors is the height of the wire above the bottom of the box. The next result is introduced to study the effect of the height of the line. A current source feeds the line at 0.1 m from the open-circuit port. In addition, a 50 Ω load is connected at the other (right) end of the line. The wire radius is varied so that the characteristic impedance of the transmission line is always 100 Ω. Fig. 21 shows a comparison of the voltage at the open-circuit port for different heights of the line above the bottom of the box. Also included is a result using transmission line theory (this result is independent of h). For the largest value of h (3 cm), a result is also included for which an infinite ground plane was assumed, with no box. The numerically-exact (full-wave) results were obtained by meshing the transmission line wire, and using a cavity Green's function to account for the presence of the cavity in a moment-method solution (Sharpe et al., 1998). The results show that the voltage calculated by the full-wave solution with h =1 mm agrees very well with that calculated by transmission-line theory. As the height gets larger, there is greater disagreement between the numerical full-wave result and the transmission-line theory result. The resonant effect of the box also becomes stronger as the height increases. At a 3 mm height, the numerical result completely disagrees with transmission-line theory. Comparing with the case for no box (infinite ground plane), the resonant effects of the box are seen clearly for this height. The result for the line above the infinite ground plane shows only a wire resonance while in the box the line shows both a wire resonance and cavity resonances. The unloaded box resonance frequencies are 0.48, 0.56, 0.61, and 0.75 GHz. The effects of the box resonances are more obvious as the height h increases. At a

3 mm height, the numerically-exact result shows very pronounced resonance peaks. From these validation results, it can be concluded that the height of a PCB transmission line (i.e., the thickness of the substrate) should not exceed about 5 mm in order for the hybrid method to provide accurate results for the range of frequencies considered. The following results all assume a height of $h = 1$ mm.

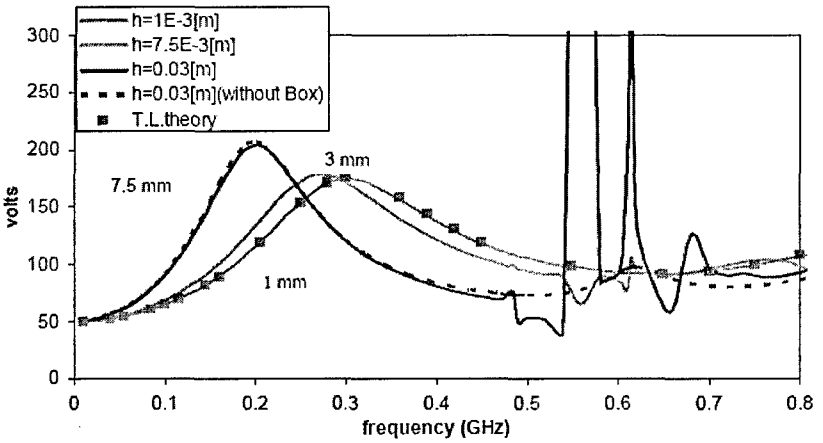

Fig. 21. Magnitude of the voltage at the open-circuit port for different heights h of the wire above the bottom of the box.

2) Time Domain Results due to a Plane-wave Pulse. Time-domain coupling from an incident plane-wave pulse to a device on a printed circuit board inside of a metallic cavity enclosure is calculated and studied, using an efficient hybrid method. The cavity has an exterior feed wire that penetrates through an aperture and makes direct contact with the printed-circuit board trace that leads to the device. The signal level at the input port of the device is calculated and studied. The incident electromagnetic field is assumed to be a time-domain plane wave in the form of a pulse, and two pulse shapes (a Gaussian pulse and an exponentially damped sinusoidal pulse) are studied. Results show how different pulse characteristics produce different types of signals at the input to the device. The time-domain results are validated by comparing with simple expressions based on the resonant frequencies and Q of the cavity.

The modulated Gaussian pulse is shown in Fig. 22a and the damped sinusoidal pulse is shown in Fig. 22b.

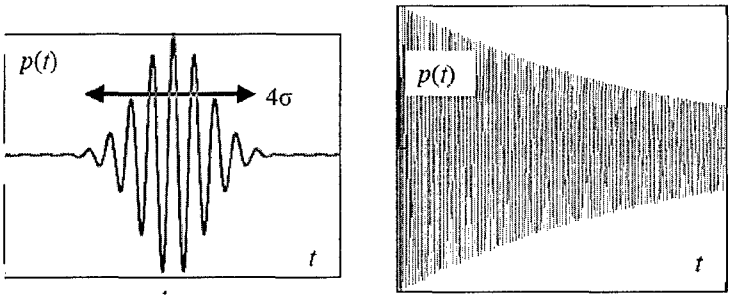

Fig. 22. Pulses under investigation. (a) Gaussian pulse. (b) Damped sinusoidal pulse.

a) Modulated Gaussian pulse. The pulse has the center frequency of 0.35 GHz. The decay parameter σ is chosen as 9.66E-9 s and the corresponding bandwidth is 0.28 GHz. The open-

circuit port voltage is calculated numerically. Fig. 23 shows the output (port) voltage and the input (signal) voltage for comparison. Also shown is an envelope that is obtained by shifting the envelope of the input signal by the group delay. As expected, the output signal has the form of (11). That is, the output signal is a scaled version of the input signal, with the carrier shifted by the phase delay and the envelope shifted by the group delay. A calculation shows that the group delay of the output signal is about -7.027E-10 s so that the envelope of the output signal is advanced by 7.027E-10 s, while the phase delay of the output signal is about 8.347E-10 s. Fig. 23 shows good agreement with these calculations, although the shift in the envelope is difficult to see on the scale of the plot. An expanded scale (not shown here) verifies that the envelope of the output signal does match well with the shifted envelope of the input signal.

b) The damped sinusoidal pulse. The pulse is centered about the (011) cavity mode resonance. The pulse has the center frequency of 0.51 GHz, the same as the center frequency of the cavity resonance. Two different values of the signal quality factor Q are used. One value is greater than the Q value of this cavity mode and the other is smaller. The two values of Q are 510 and 51. Recall that the value of Q_c of this cavity mode is 128. Fig. 24 shows the output signal as well as the envelope functions corresponding to the input signal and the cavity response. Fig. 24 shows results for the high-Q signal. Both the input signal and the cavity response are in the form of exponentially decaying sinusoidal waves. However, because the Q_s of the signal is much larger than the Q_c of the cavity, the late-time response of the system is dominated by the Q_s of the signal. Hence, for late time it is seen that the envelope of the output signal matches quite well with the envelope of the input signal.

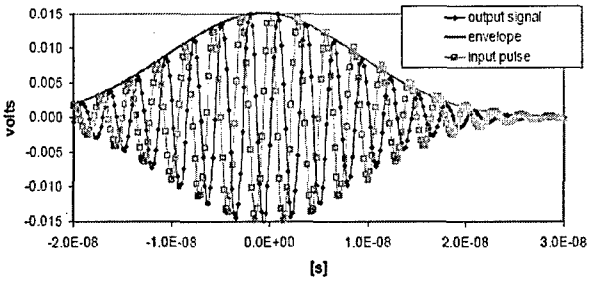

Fig. 23. The open-circuit port voltage excited by Gaussian pulse.

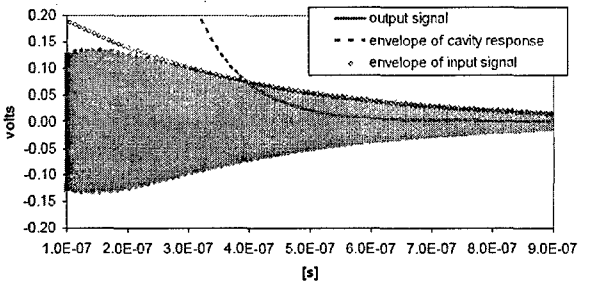

Fig. 24. The open-circuit port voltage excited by damped sinusoidal pulse with $_s Q$ =510.

2.4) THE OHIO STATE UNIVERSITY AND UNIVERSITY OF MICHIGAN

EMI/EMC team at The Ohio State University has taken a broad multi-disciplinary approach to address the fundamental aspects of RF-MURI project. Our research has primarily focused on developing theoretical tools for large class of EMI/EMC problems including EM structures, cable bundles and mixed-signal circuits. We also conducted measurements using realistic platforms to provide reference data to other research teams of our MURI.

1) Our early focus was on developing fast computational EM tools to address large structures with high computational efficiency. Therefore, we customized our own Multilevel Fast Multipole Method (MLFMM). We also improved our Finite Element Boundary Integral (FE-BI) tool to optimize its use for PCB structures. Subsequently, we have successfully employed FE-BI

in conjunction with Agilent's Advanced Design System (ADS) to investigate EMI effects on RF circuits. We further developed optimization tools such as DIRECT with Kriging Meta model and employed them for realistic problems such optimum location for microcontrollers in an automobile platform for minimum EMI interference. Examples of are shown in Figs. 25 and 26.

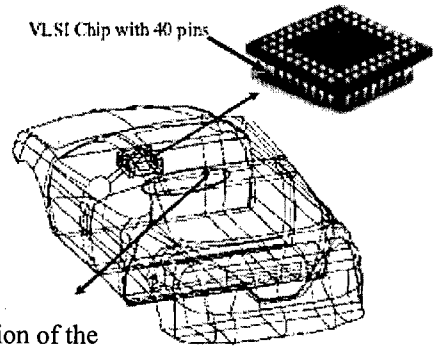

Fig. 25. Geometry of optimization problem for minimal EM coupling from the source antenna to 40 pins on a very large scale integration (VLSI) chip.

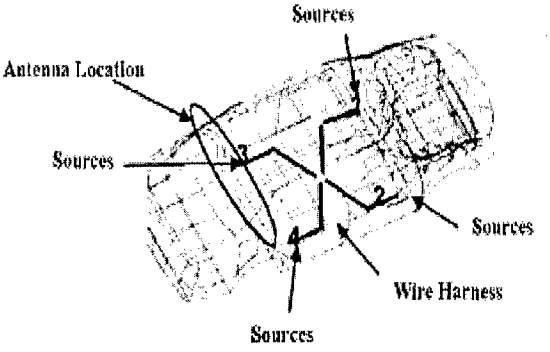

Fig. 26. Geometry of the EMI coupling reduction problem. Optimized antenna location is also shown.

2) In parallel to developing numerical EM tools for large structures and PCBs, we have also improved existing transmission line tools to account for non-static contributions in cable bundles. We derived Telegrapher's Iterative Coupling Equations (TICE) and validated them for various complex platforms such as trough and cavity-like structures. TICE is not only suitable for rigorous analysis of non-uniform cable bundles in complex platform but it also accommodates analysis of linear/nonlinear electronic modules (compatible with SPICE) attached to the cable bundles. To reduce the computational cost involved in iterative analysis of cable bundles, a current decomposition approach was developed. This unique current decomposition approach allowed analyzing the bundle-to-surrounding structure coupling via full wave solvers while tackling the interactions within the bundle via Transmission Line Theory.

We propose a new approach employing a current decomposition method for mass transmission line bundles near the complex structures. Under the proposed method, the current on each transmission line is decomposed into push-push (average) and push-pull (perturbation) mode currents (as shown in Fig. 27). A similar convention was used by Schelkunoff and Friis for the analysis of two wire antennas in free space. The former accounts for the interactions between the surrounding structure and the transmission lines, and the latter is responsible for the current perturbation due to interactions among the transmission lines forming the bundle. The push-pull mode current is computed via the traditional transmission line method by taking one of the transmission lines in the bundle, preferably the one at the center, as return/reference conductor. To evaluate the push-push mode current, we compute the current of a test wire located along the reference transmission line in the presence of the surrounding structure. SPICE models are then employed for the push-pull mode current to analyze the equivalent coupling circuit models extracted via PEEC.

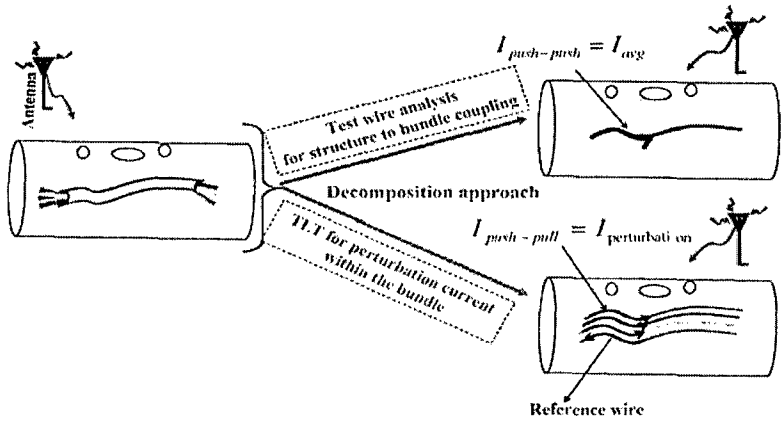

Fig. 27. Current decomposition approach for transmission lines in the presence of complex structures.

To validate the proposed method in complex structures, we consider the geometry in Fig. 28. Specifically, we consider 5 wires and the whole structure is illuminated by a plane wave at 0.3GHz. Failure of the conventional MTLT for highly complex structures is easily substantiated in this example as shown in the results in Fig. 28. We observe that the proposed method agrees very well with rigorous data even for highly non-static contributions.

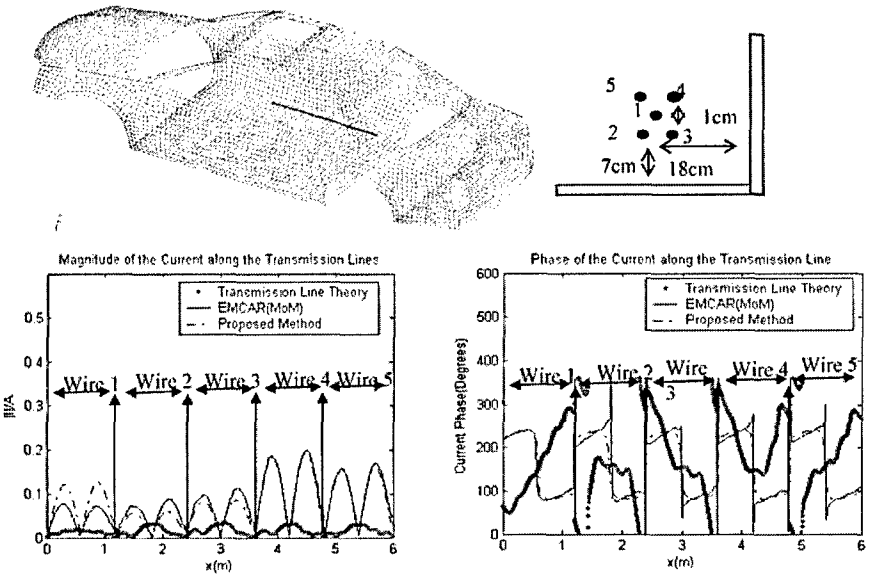

Fig. 28. Five transmission lines inside an automobile illuminated by plane wave and total current induced on each transmission line.

3) For perforated cavities, we developed semi-analytical tools based on dyadic Green's function formulation using Kummer transformation in conjunction with the Poisson sum property. These semi-analytical tools were combined with CRIPTE to address field coupling to cable bundles inside cavity-like structures. Further, we improved our semi-analytical tools to

model multi-layer circuits within cavities. Moreover, a rigorous analysis of the wires inside cavities was done with Moment Method approach. However, to address the numerical bottleneck encountered with rigorous computational analysis, an iterative algorithm was employed for the analysis of Printed Circuit Boards (PCBs) in conjunction with wires inside cavities.

To validate the technique, coupled voltage is computed at the 50Ω load of inter-digital filter enclosed within a rectangular cavity having a slot illuminated by E_y polarized plane wave incidence. The details of all dimensions are given in Fig. 29. The present method (Magnetic Green Function) is compared with HFSS (Ansoft) and electric MoM-Green function method using electric currents in the metallic parts of the layer interface. In all cases, close agreement is exhibited for broad frequency band. We observe two large coupling peaks at around 2GHz and 6 to 8 GHz, corresponding to the resonances of the filter and the cavity plus aperture.

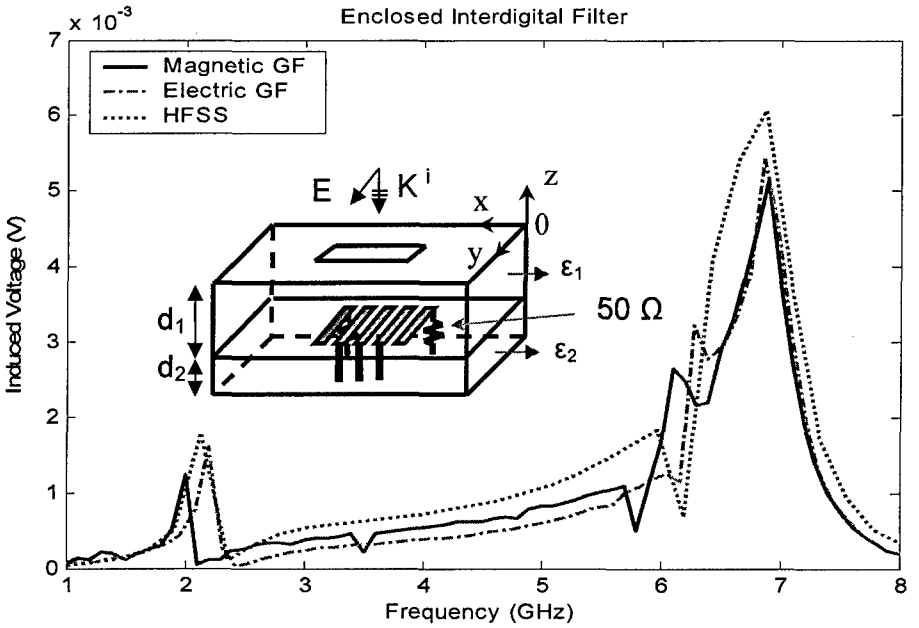

Fig. 29. Voltage at the load of an inter-digital filter enclosed a cavity. The dimensions are given as follows: cavity (29 x 40 x 4), aperture (19 x 2), strip (1 x 20), d_1=1, d_2=3, ε_1=1, ε_2=3.48 in [mm].

4) Recently, we also developed a hybrid S-parameter matrix method for combining full wave solvers with circuit tools such as HSPICE and ADS to analyze EMI/EMC effects on mixed-signal circuits. We used the hybrid S-parameter method to investigate high power EMI effects on an inverter shielded by a box. The same method was employed for more complex and practical EMI/EMC problems including RF-power amplifiers and a timer in presence of complex platforms.

We also teamed with Prof. Roblin's research group at The Ohio State University to understand and characterize EMI effects on RF circuits and communication systems. Specifically, we carried out measurements on an in-house designed RF power amplifier with Large Signal Network Analyzer (LSNA- obtained via an AFOSR Grant in 2004). EMI effects on the performance of the RF-amplifiers were studied using different pulse rates and modulations. In this context, the constellation diagrams of coding schemes were used to determine bit error rates. The type of realistic system characterization has allowed stressing our computational tools

in addition to providing a platform for practical understanding of EMI effects on mixed analog-digital systems.

For RF-digital systems, a challenge is the integrated analysis of circuit elements (the governing equations being the -Kirchhoff's Voltage (KVL) and Current Law (KCL)) with EM structures governed by Maxwell's equations. While the former is expressed in terms of voltages and currents, the latter requires the solution of electric and magnetic fields. Due to the inherent non-linearities of the analog and digital circuits having varying input and output impedances, it is impractical to integrate both into a full wave EM solver in the frequency domain. Therefore, EM structure either needs to be transformed into a circuit compatible form via, for instance, Partial Element Equivalent Circuit (PEEC) method or port analysis via S-Parameter network characterization. We extended the port analysis technique to accommodate the external plane wave coupling. In other words, we proposed a frequency domain method which overcomes the CPU bottleneck of time domain techniques and concurrently yields increased accuracy as compared to MTLT. As part of this formalism, we introduce additional hybrid S-parameters to establish a link between the existing board ports and external plane waves (see Fig. 30).

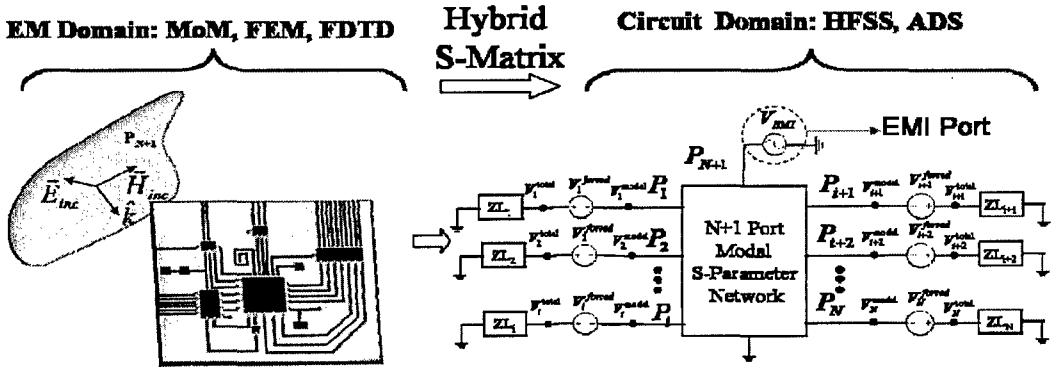

Fig. 30. Hybrid S-parameters to represent external EMI.

In addition to additional entries in S-matrix to represent plane wave excitation, we also introduced forced voltage sources at the port locations to enforce the Ohm's law at the ports. Having characterized plane wave as a part of the S-matrix, we can handle both on-board and offboard EMI problems simultaneously. This approach can be easily integrated into circuit solvers such as HSPICE and Advanced Design System (ADS, Agilent Technologies). This is achieved by exporting new hybrid S-parameters. The method allows both time domain simulations via broad band network characterization and Harmonic Balance Simulation of non-linear RF components. We present EMI effects on the TI SN74AUC1GU04 inverter residing on a RT/Duroid 5870 board inside a metallic enclosure with effective dielectric constant of 2.33 and thickness of 31 mils (see Fig. 31). We first generated a 8x 8 S-Parameter matrix for the ports in the absence of the plane wave. Next, the proposed method is employed to compute the hybrid S-Parameters. Subsequently, we updated the existing S parameter matrix to include the hybrid parameters and generate a 9×9 S-parameter network. As a final step, we exported the resulting matrix into HSPICE and performed a time domain analysis. Fig. 31 shows the inverter output for three different cases. In the first case, no EMI was applied and it is clearly seen that the inverter performed as expected. In the second case, an external field of amplitude 1414 V/m was applied, resulting in minor oscillations at the output. However, when external EMI was doubled,

2828V/m, EMI effects began to dominate, resulting in significant modifications on the output. This example also implies that even though inverter was shielded, a small aperture cut-out for input and output cables may lead to severe coupling to the device, and eventually to logic failure.

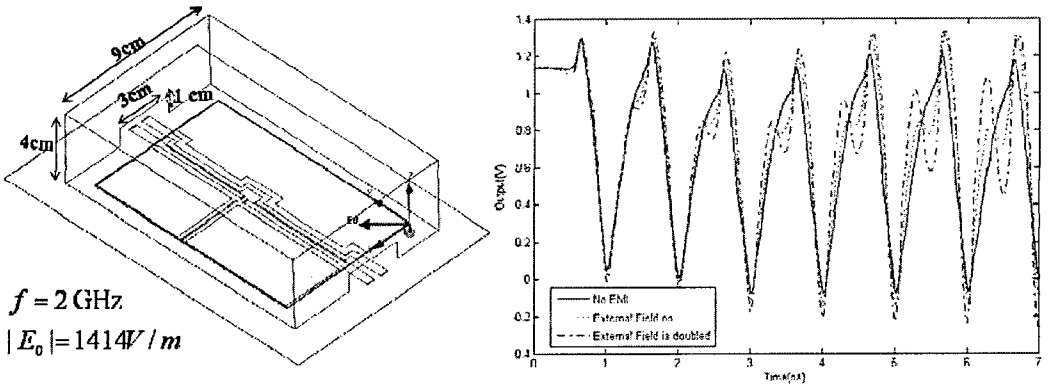

Fig. 31. Inverter inside a metallic box and subject to concurrent on & off-board excitation.

5) We have also collaborated with Prof. Iliadis' group at University of Maryland to characterize EMI effects on Digital Circuits, particularly on a Timer used to control spark plug sequence in automobiles. An example is shown in Fig. 32. For this effort, we designed an in-house timer and manufactured it using a MOSIS 0.5μ line. In addition to performing measurements to observe circuit-level effects, we also performed theoretical analysis for a timer board located inside a GM Deville car to characterize interfering signal in terms of pulse width and length as well as incidence angle for different failure mechanisms. Such analysis required integration of full wave solvers and circuit tools via our recently developed hybrid S-parameters method. Several papers were prepared based on this method.

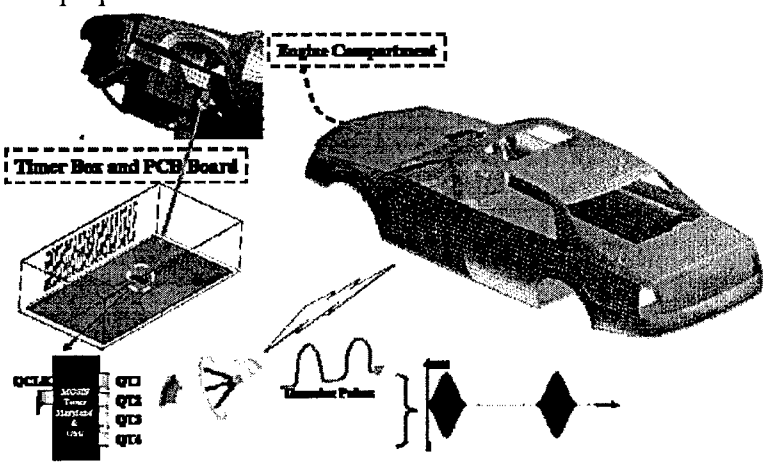

Fig. 32. A timer inside an Automobile subject to HPM.

Referring to the measurement setup in Fig. 33(a), the EMI is injected via a hybrid power combiner connected to the clock signal as well. The timer has 11 decoded outputs (*O*0 - *O*9 and *O*5*j*9), active clock inputs (*CP*1, *CP*0), and a master reset input (MR). It is designed to advance with positive or negative edge trigger depending on the pin connections of the clock and master reset inputs. For our experiments, MR and *CP*0 were set to logic low and high respectively to

provide negative edge clock trigger at the *CP*1 clock input. An HP8116A 50MHz pulse function generator was used to generate the clock pulse signal. EMI signal was obtained via an HP 8753C 300kHz -6GHz network analyzer set. To investigate interference effects on the timer, the clock pulse and EMI signal were connected to the *CP*1 clock input port through the power combiner and the decoded outputs were then measured using Tektronics 450 digital oscilloscope. In other words, the measurement was setup in a way to investigate the impact of disrupted clock signals on the timer performance. The oscilloscope was connected to a computer controlled by Labview program to obtain experimental data. The counter was biased with 2V or 3.3V DC and the power and frequency of the interference signal ranged from 0 to 23dBm, and 1 to 3GHz, respectively.

The decoded output (*O*7), without EMI is given in Fig. 33(b) for a 2V DC bias and 3.4MHz clock pulse having 50% duty cycle applied to the VCC and *CP*1 port respectively. As displayed, the output had 320ns width and 2.936*s* periods indicating that the counter is at normal operation with 26ns propagation delay. To observe the interference effects, 23dBm signal at 1GHz was combined to 3.4MHz clock pulse using the combiner and applied to the *CP*1 port.

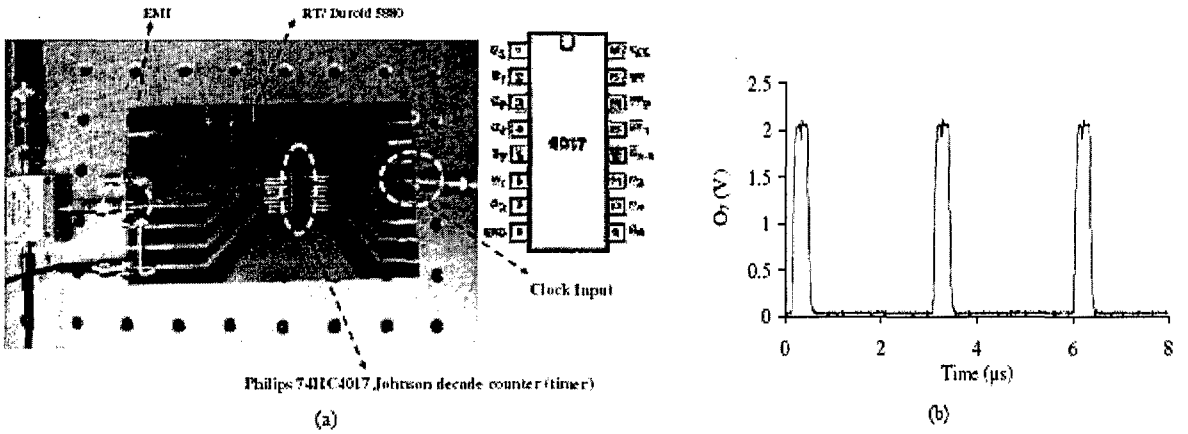

Fig. 33. (a) Measurement Setup to Examine EMI effects on Performance of Philips 74HC4017 Johnson Decade Counter (timer) - (b) Output of Johnson Timer at Port O7 with no EMI.

Fig. 34(a) displays voltage saturation level at the VCC implying that the device can not turn off the output (O7) (viz. critical device error). The voltage level also changes with respect to time as well. This demonstrates that the interference power severely degrades the device performance by invalidating the negative edge trigger of the clock signal at the port. From the device data sheet, it is noted that the port front is a CMOS inverter. Therefore, the device upset can be attributed to the changes of input/output voltages and the increase of propagation delays in CMOS inverters. After the EMI was terminated, the device returned to normal operation implying no permanent failure. Thus, this indicates that the upsets were soft errors. When the interference was at 3GHz, the timer displayed a gradual degradation at the output pulse level as the power was increased. This is seen in Fig. 34(b), where the device becomes less immune to the interference at 3GHz, which most likely is due to less EMI power reflected at 3GHz than at 1GHz, as observed with S-parameters measurement. At 20dBm, the output pulse level drops to 1.14V sufficient to cause malfunction (see Fig. 34(b)). The relationship between interference and bias voltage was also investigated. Specifically, the bias voltage was increased to 3.3V while

other inputs remained the same as before. We observed that the output pulse showed no changes with respect to the power and frequency of interference signal. Therefore, we concluded that the device becomes more vulnerable to interference as the bias voltage decreased. This is likely due to increase in delays in CMOS device as bias voltage decreases.

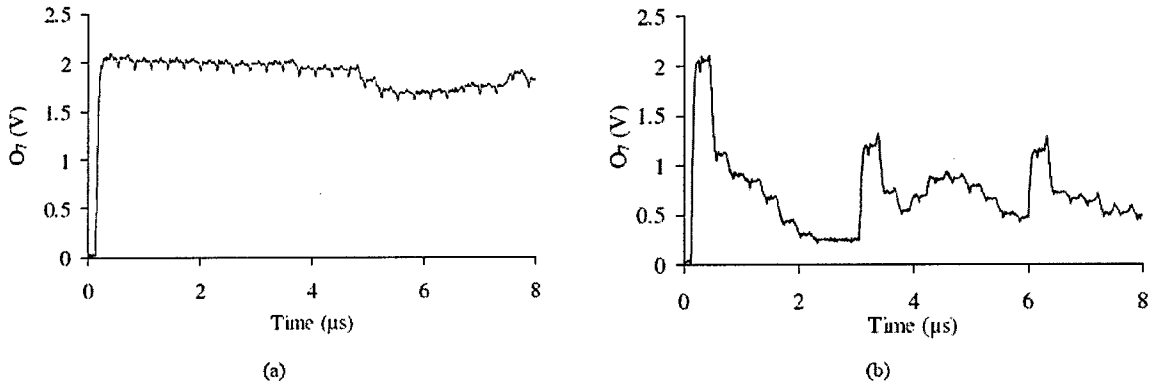

Fig. 34. (a)Output of Johnson Timer at Port *O7* Subject to 23dBm EMI signal at 1GHz - (b)Output of Johnson Timer at Port *O7* Subject to 20dBm EMI signal at 3GHz.

6) We have also combined our efforts with resources at The ElectroScience Laboratory to carry out measurements for a large metallic cavity enclosing additional smaller rectangular and cylindrical cavities, cables and circuits, and subjected it to external electromagnetic interference. The collected measurements were reported at conferences and were directed at validations of analyses carried out at Ohio State/Michigan, Clemson (Prof. Butler) and Houston (Prof. Jackson and Prof. Wilton).

Fig. 35 shows the multi-cavity structure, enclosing cylindrical and rectangular cavities. Two cables penetrate the enclosure through apertures and each end in a smaller cavity. One cable is directly connected to a printed circuit board placed in the smaller rectangular cavity. A PCB layout (which is in fact a matching network) is also given. The cylindrical cavity encloses a coaxial cable with a small section of shielding removed to allow field coupling onto the interior conductor. Fig. 36 gives our first coupling measurements when the multi-cavity structure is empty. The field is measured at the center of the left or right cavity. As seen, the coupling data compares well with the Moment Method calculations. However, the simulations could not converge at resonances justifying the need for a more efficient solver especially when cables and PCBs will also be present inside the cavity. Fig. 37 presents EM coupling to a PCB interconnect when the penetrating cable is directly attached with the PCB trace. For one set of measurements, the PCB is enclosed only by the smaller rectangular cavity and for the other, the PCB and the smaller rectangular cavity were placed inside the cascaded cavity. It can be observed by comparing the results that that once the cable is attached directly to the PCB, increasing the level of shielding show no significant improvement to EMI coupling at higher frequencies.

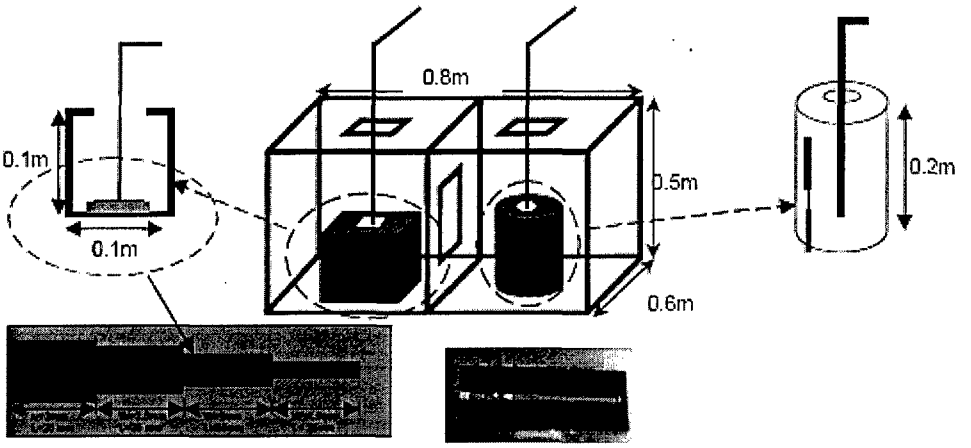

Fig. 35. Cavities and PCB used for measurements.

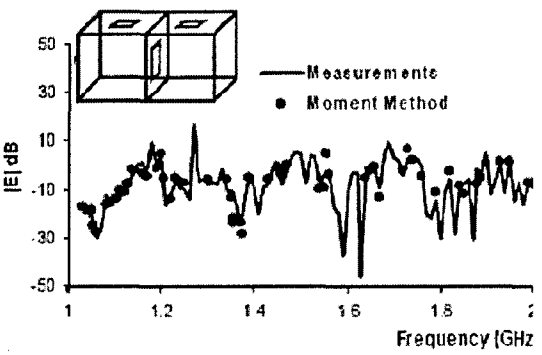

Fig. 36. Field Strength at the center of left section of the empty enclosure.

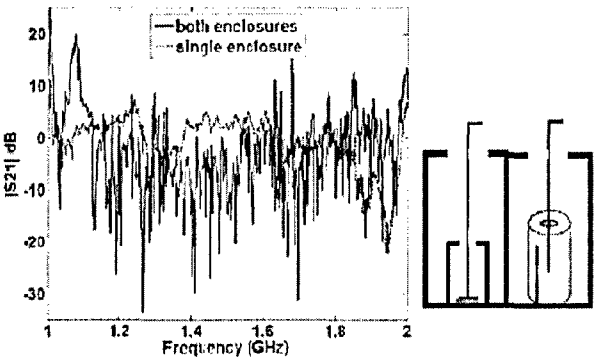

Fig. 37. Coupling to PCB inside smaller rectangular cavity.

We are currently undertaking a research effort that expands upon our hybrid S-parameters approach to combine both cable bundles and mixed-signal circuits under a single matrix system that can be combined with HSPICE or ADS in conjunction with full wave solvers such as EMCAR (MLFMM code developed by our team) for system level analysis.

2.5) UNIVERSITY OF ILLINOIS AT URBANA-CHAMPAIGN

A novel, fast and comprehensive time-domain method for analyzing electromagnetic compatibility and interference (EMC/EMI) phenomena on complex structures that involve electrically large platforms (e.g., vehicle shells) along with cable-interconnected antennas, shielding enclosures, and printed circuit boards, was developed. To efficiently simulate field interactions with such structures, three different solvers were hybridized.

(i) *A time-domain integral-equation based field solver that computes fields on the exterior structure comprising platforms, antennas, enclosures, boards, and cable shields (external fields).* This field solver rigorously solves time domain electric and combined field integral equations by marching on time and incorporates stable new time stepping schemes that are stable even when applied to the analysis of very large and structures discretized using irregular meshes. The solver

models perfectly conducting, resistive, and impedance surfaces, wires, and dielectric volumes. Some examples are shown below.

The first geometry considered consists of a thin metallic strip mounted on a flat rectangular PEC plate (see Fig. 38). The geometry is fed by a 50- coaxial transmission line; the source point on the transmission line resides 2.5 cm below the bottom edge of the strip. For this structure, radiated power was measured and reported for the frequency range of 0–2 GHz. The geometry is modeled using spatial unknowns. The current and the voltage at the source point are recorded during the simulation and the radiated power as a function of frequency is computed accordingly. As seen in Fig. 39, the measured and numerical results obtained using the MOT-PWTD codes are in very good agreement.

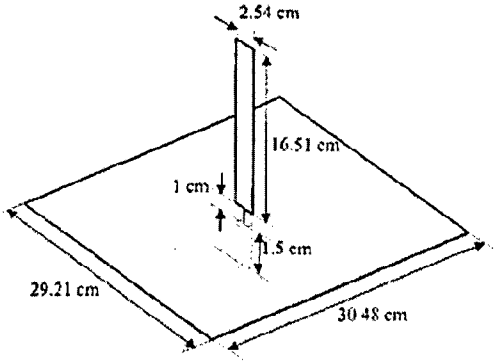

Fig. 38. Narrow strip mounted on flat rectangular plate.

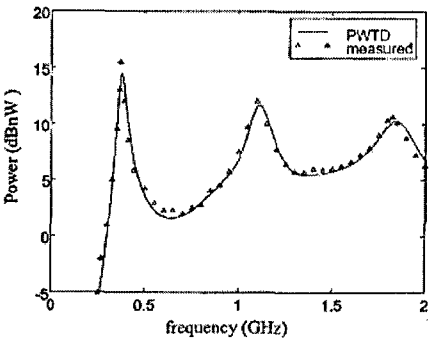

Fig. 39. Radiated power by the narrow strip on a flat plate.

Next, a more challenging problem is considered as the resonance frequencies of a rectangular PEC box loaded with a wire (see Fig. 40) are calculated. The wire is the 0.8-mm radius inner conductor of a 50Ω coaxial line with a 50Ω source resistance, connected to the top of the box. The wire is terminated at the bottom of the box with a 47Ω resistor. For this structure, the power delivered by the source as a function of frequency was measured and reported. The same problem is analyzed using the MOT-PWTD algorithm. The geometry is discretized by 5800 spatial unknowns. A delta-gap voltage source is placed in the wire/box junction to model the excitation with the waveform specified by (28) with GHz and s. The 47Ω load resistor is modeled as a lumped resistive element in the MOT-PWTD algorithm. The algorithm was run for 10 000 time steps. Because this is a resonant structure and because we are only interested at the current values at the source point, this large number of time steps can be avoided by extrapolating all pertinent current waveforms using one of the well-known transient extrapolation methods, e.g., Prony's method, the generalized pencil-of-function method, or one of the variants of the autoregressive (AR) method. It should be noted that, at least for this particular example, four- to fivefold savings in the total simulation time can be achieved by using such a scheme in conjunction with the MOT-PWTD solver. The total power delivered by the source as a function of frequency is plotted in Fig. 41. The MOT-PWTD algorithm correctly predicts the locations of all the resonant frequencies.

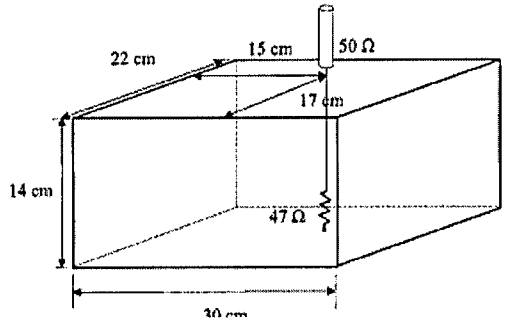

Fig. 40. PEC box loaded with a wire.

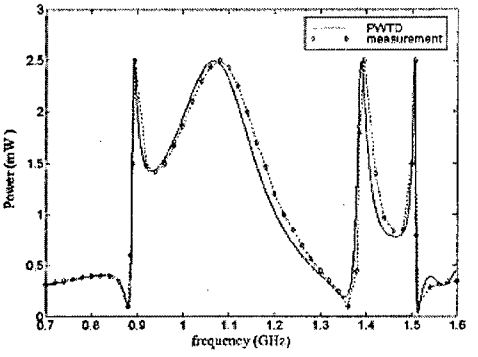

Fig. 41. Power delivered by the source for the PEC box loaded with a wire.

A problem of interest to many EMC engineers involves the characterization of the EMC/EMI properties of board/card configurations on personal computers or related equipment. Within this context, our final example consists of PEC models of a motherboard, a source card, and a shielding card (with eight pins) enclosed in a rectangular shielding box with a slot (see Fig. 42). A delta-gap source is placed at the point where the source card is connected to the motherboard. The MOT-PWTD algorithm is used to analyze the shielding effectiveness of the shielding card and the enclosing box. The entire structure is modeled in terms of 7600 spatial unknowns. The excitation pulse is of the form of

$$V^{exc}(t) = V_0 \cos(2\pi f_0 (t - t_p)) \exp(-(t - t_p)^2 / 2\sigma^2) \qquad (1)$$

where $f_0 = 1.25\,\text{GHz}$ and $\sigma = 1.91 \times 10^{-9}\,\text{s}$. First, the frequency dependent radiation impedance of the structure without the enclosing box is computed from the time-domain voltage and current values at the source point. This data is compared to that obtained using the aforementioned MOM code. The agreement between the two sets of results is very good (see Fig. 43).

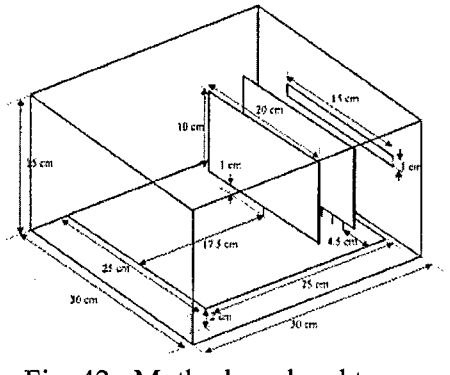

Fig. 42. Motherboard and two cards placed in a closed box with an aperture.

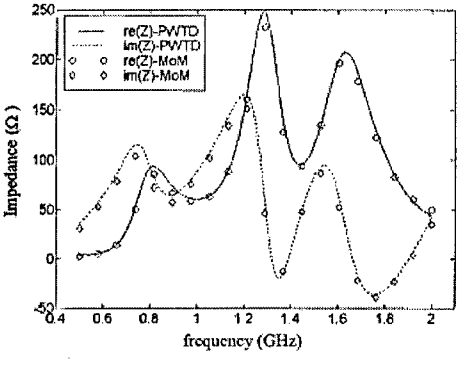

Fig. 43. Impedance seen by the source.

(ii) *A modified nodal-analysis based circuit solver that computes currents and voltages on lumped circuits approximating cable connectors/loads.* This "SPICE-like" solver handles

arbitrarily complex networks of linear elements (resistors, capacitors, and inductors) and incorporates a limited database of nonlinear elements.

The microwave amplifier shown in Fig. 44(a) has been previously analyzed using the FDTD and FETD methods. Here, the same amplifier is analyzed using the hybrid field-circuit simulator developed in this project. The problem geometry is modeled using PEC microstrip lines that reside on a finite dielectric substrate backed by a conforming finite PEC ground plane. The lumped circuits in the problem comprise of a nonlinear MESFET that resides at the center of the structure and the linear termination networks at the input and output ports [see Fig. 44(a)]. The large-signal circuit model for the MESFET is shown in Fig. 44(b). Note that this particular circuit representation is based on the Curtice–Cubic model. The input and output ports are both terminated with lumped 50Ω resistors. In what follows, first, the amplifier is simulated without the shield and the calculated -parameters are compared to those obtained using HP ADS. Next, the shield is included in the simulation, and for a number of different shielding geometries, the change on the s-parameters is examined. Finally, the shielding effectiveness of the structure to EMI due to various external excitations is investigated by observing transient waveforms at various ports in the system.

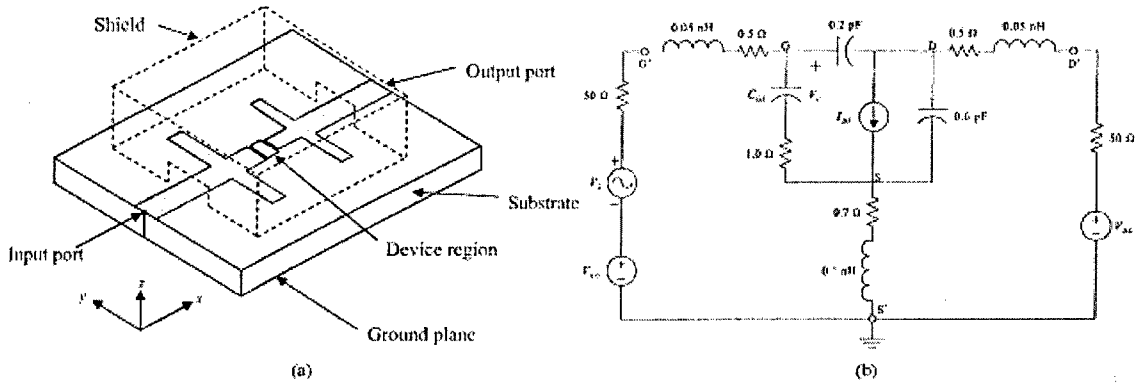

Fig. 44. (a) Microwave amplifier with shielding structure. (b) Circuit model of the MESFET.

To calculate the s-parameters of the microwave amplifier without the shielding structure, two different spatial meshes corresponding to ground plane sizes of 690×640 mm and 960×650 mm, are constructed. Both meshes support frequencies up to 10 GHz. The resulting number of electromagnetic unknowns is 5269 and 8564, respectively. The voltage at the input port is supplied by a delta-gap source with a modulated Gaussian temporal signature shown in Fig. 1, where $f_0 = 6\,\text{GHz}$, $\sigma = 3/14\pi\,\text{ns}$, and $t_p = 6\sigma\,\text{s}$. The amplitude of the input pulse is chosen sufficiently small such that the MESFET operates in the linear regime. In all simulations presented herein, the time step size is 5 ps. The dc operating point of the MESFET is chosen as $V_{G'S'} = -0.81$ V and $V_{D'S'} = 6.4$ V. The s-parameters calculated at the source and load points by the hybrid field-circuit simulator are compared with HP ADS results in Fig. 45. The agreement between the two sets of data is satisfactory. The largest discrepancy is in the data at frequencies above 7 GHz, which could be due to a number of factors, including the particular -parameter extraction method utilized. A more accurate way to determine s-parameters is to calculate the incident and reflected waves on the input and output microstrip line sections using de-embedding techniques. It is interesting to note, however, that the size of the finite ground plane has little to

no effect on the s-parameters for the two cases considered here (in Fig. 45, EM-CKT1 and EM-CKT 2 correspond to ground planes of size 960×650 mm and 690×640 mm , respectively).

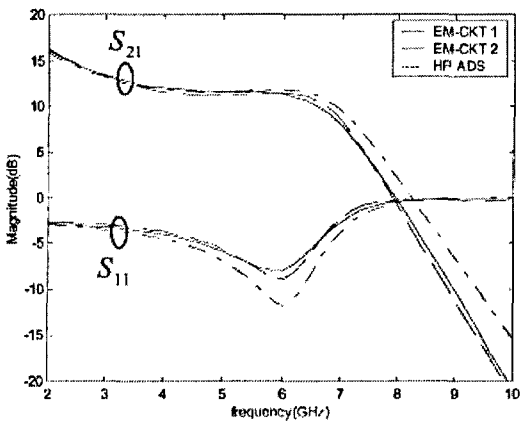

Fig. 45. S_{11} and S_{12} of the amplifier without a shield.

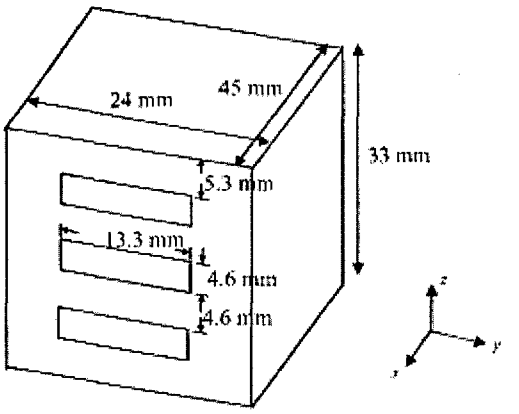

Fig. 46. Dimensions of a large PEC enclosure.

In the final example, the amplifier is placed at the center of a larger PEC enclosure that contains three equally sized holes on one side of the enclosure shown in Fig. 46. The incident plane wave has the parameters $f_0 = 4\,\text{GHz}, \sigma = 1/(4\pi)\,\text{ns}$, $E_\theta = 500\text{V/m}, \theta_i = 135^0, t_p = 0.5\text{ns}$, $E_\phi = 500\text{V/m}$, and $\phi_i = 180^0$.

The overall geometry has been discretized using 17927 basis functions. The voltages at the input and output of the transistors in this case are shown in Fig. 47(a) and (b), respectively. The above examples illustrate a simple scenario where the EMI from external sources is modeled using a plane-wave excitation model. It is also assumed here that the aforementioned large-signal model for the MESFET remains valid for all of the above excitations. A careful examination of the magnitude of the voltages at the input and output ports of the transistor and comparison of the MESFET model to that of the original Curtice–Cubic model has revealed that this assumption is indeed true for all the cases considered here. In most real-life scenarios, the EMI source can be a lot more difficult to identify and more complete device models may need to be incorporated into the solution scheme. Nonetheless, the results presented here still demonstrate the capability of the proposed hybrid field-circuit simulator to analyze such problems in an efficient and accurate way. The reduced computational complexity of PWTD-accelerated MOT-based field solvers has been demonstrated previously in the literature by experimentally verifying the asymptotical scaling laws for these algorithms. Here, we concentrate on simulation of a specific geometry to assess the computational efficiency of the proposed hybrid field-circuit solver. The number of electromagnetic and circuit unknowns for this geometry are 5269. There are two nonlinear circuit elements [i.e., the nonlinear current source and the nonlinear capacitor in Fig. 47(b)]. Analysis of this geometry for 500 time steps using a time step size of 5 ps requires 35 min of CPU time on a 2.4-GHz Pentium IV PC operating on the Linux platform. Note that all the other simulations performed in this study to generate the results presented require very similar computational resources.

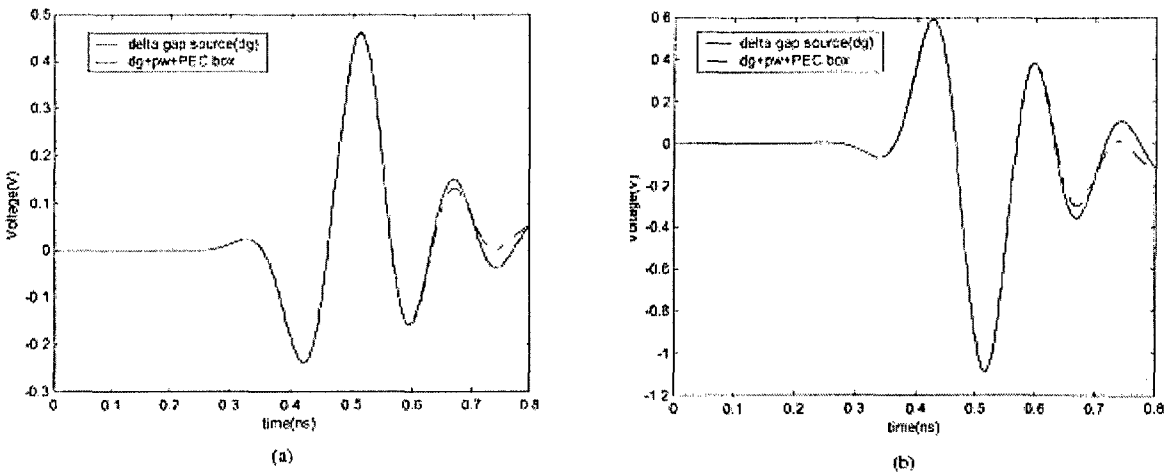

Fig. 47. Time-domain response at: (a) input and (b) output of the transistor for $\theta_i = 135^0$ and $\phi_i = 180^0$.

(iii) *A time-domain integral-equation based transmission-line solver that computes transmission-line voltages and currents at cable terminations (guided fields).* The method computes fields on complex and multi-scale structures, including platform installed shielding enclosures, antennas, printed circuit boards, coaxial cables, and cable connectors/loads by employing three different solvers: (i) a time-domain integral-equation based FFT accelerated parallel field solver, (ii) a finite-difference time domain based cable solver, and (iii) a modified nodal analysis based circuit solver. These solvers are coupled at the cable connectors/loads and shields; the resulting *coupled* system of equations is solved *simultaneously* at each time step. The proposed method is used to analyze cable-induced coupling to PC cards located in a shielding enclosure.

An RG-11 coaxial cable of length L = 5 m with outer shield radius a = 3.7084 mm, characteristic impedance Z_c=75Ω and internal wave speed $c_{CBL} = 2.33\times10^8$m/s is terminated by two resistors R_1=50 Ω and R_2=120 Ω (Fig. 48(a)). The cable shield's transfer impedance function is $Z^{CBL}(f)$=4+$j2\pi f$0.25×10−6 mΩ/ m. The cable, which resides in free-space and extends along the x- direction, is illuminated by an x- polarized modulated Gaussian plane wave propagating in z- direction (Fig. 48(a)). The common-mode current density on the cable shield, the differential-mode current, and the load voltages are represented by N_{EM} =101 wire basis functions, N_{CBL} = 101 FDTD current samples, and N_{CKT}= 2 circuit unknowns, respectively. The simulation is carried out for 2,500 N_t = time steps of duration Δt =0.21 ns and the time-domain voltage $V(t)$ at point 1 (Fig. 48(a)) is recorded. The frequency domain voltage at point 1 is also computed by using the following semi-analytical expression. Fig. 48(b) compares frequency domain voltage obtained by using this procedure to that computed by the discrete Fourier transform of $V(t)$ divided by the Gaussian shape function. The good agreement in Fig. 48(b) verifies the accuracy of the FDTD solution, and the coupling of cable and circuit solvers.

An RG-58 coaxial cable of length L = 0.675 m with outer shield radius a =1.524 mm, characteristic impedance Z_c=75Ω and internal wave speed $c_{CBL} = 2.33\times10^8$ m/s is connected to the feed point of a PC-card configuration (Fig. 49(a)). The cable shield's transfer impedance function is $Z^{CBL}(f)$=14.3+$j2\pi f$×10−6 mΩ/ m. Of the two identical daughter cards, card 1 is

connected to the mother board with one pin at the feed point of the card configuration, whereas card 2 is connected to the mother board with eight pins.

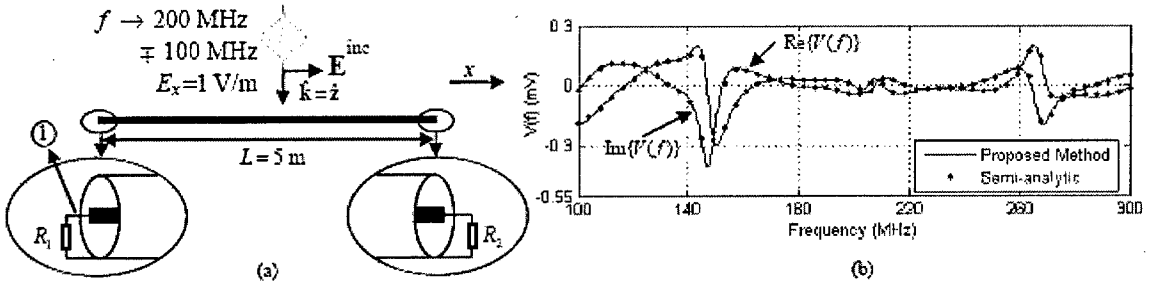

Fig. 48. Free standing RG-11 coaxial cable. (a) Geometry description and plane-wave excitation. (b) Voltage at point 1 for R_1=50Ω and R_2=120 Ω.

As an example of simulation, the voltage source is replaced by a matched load, the cards are shielded by a perfect electrically conducting box, and the whole structure is illuminated by a *y*-polarized modulated Gaussian plane wave propagating in *x*- direction (Fig. 49(a)). The simulations are carried out for 800 N_t = time steps of duration Δt =62.5 ps. The common mode current density on the cable shield and the differential-mode current are represented by 48 wire and junction basis functions and N_{CBL} = 40 FDTD current samples, respectively. The current density on the cards and the cable shield (and the shielding enclosure) is modeled with N_{EM} = 844 (N_{EM} = 2140) body, wire, and junction basis functions, and there are N_{CKT} = 9 circuit unknowns. The voltage is observed at the feed point (point 1 in Fig. 49(a), see Fig. 49(b)). The simulation (Fig. 49) quantifies coupling through an imperfectly shielded coaxial cable to an electronic system in a perfectly shielded enclosure.

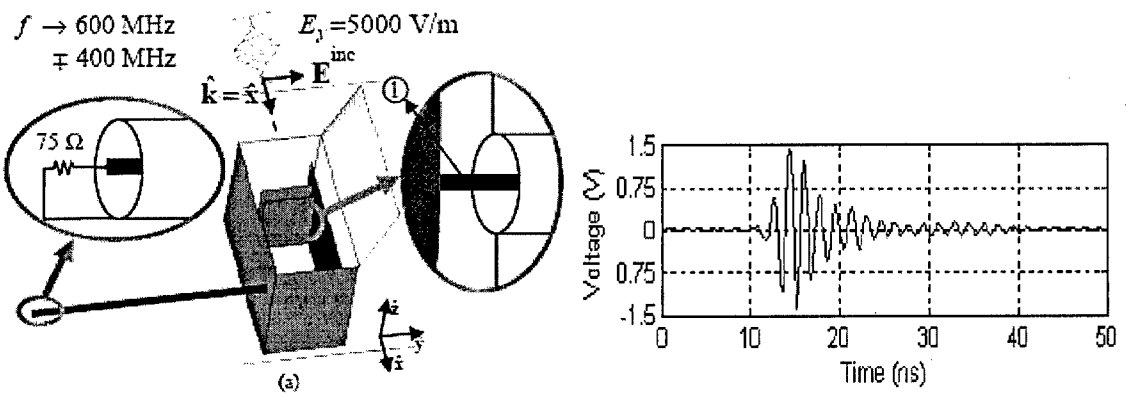

Fig. 49. Cable-induced coupling into a shielding enclosure. (a) Geometry and excitation description. (b) Voltage at point 1. (c) Snapshot of the current (in dB) at t=100 Δt. (d) Snapshot of the current (in dB) at t=250 Δt.

The aforementioned comprehensive time-domain electromagnetic modeling methodology was complemented with algorithms for the macro-modeling of both transmission-line models of

multi-wire cables and portions of the electromagnetic structure that can be defined in terms of multi-port electromagnetic networks. More specifically:
(i) A methodology was developed and an algorithm was demonstrated for the direct synthesis of macro-models of the transmission line properties of multi-wire cables given their per-unit-length, frequency-dependent, inductance, capacitance, resistance, and conductance matrices for the cable. The methodology is such that the number of state variables in the macro-model is the minimum possible. Furthermore, the macro-model is cast in terms of a SPICE-like sub-circuit and thus is directly compatible with the transient electromagnetic field solver.
(ii) A methodology was developed and an algorithm was demonstrated for the synthesis of rational function macro-models of multi-port electromagnetic structures given frequency and/or time domain data for their network transfer functions obtained either through numerical analysis or through measurement. The synthesized rational functions can be interfaced with the transient electromagnetic field solver either through recursive convolution or through their interpretation in terms of SPICE subcircuits.
These three solvers are rigorously interfaced at the cable connectors/loads and along the cable shields; the resulting *coupled* system of equations was solved *simultaneously* at each time step. Computation of the external and guided fields, which constitutes the computational bottleneck of this approach, is accelerated using fast Fourier transform (FFT)-based algorithms. Further acceleration was achieved by parallelizing the computation of external fields. The resulting hybrid solver permits the analysis of electrically large and geometrically intricate structures loaded with coaxial cables.
The accuracy, efficiency, and versatility of the proposed solver were demonstrated by analyzing several EMC/EMI problems including interference between a log periodic monopole array trailing an aircraft's wing and a monopole antenna mounted on its fuselage, coupling into coaxial cables connecting shielded printed circuit boards located inside a cockpit and coupling into coaxial cables from a cell phone antenna located inside a fuselage.
Funded by a Phase I and Phase II SBIR from AFRL (Kirtland AFB) (Program manager: Joe Yakura), the solver developed under the MURI effort currently is being extended by MURI team members Eric Michielssen, Andreas Cangellaris, and Fred Tesche in collaboration with DelCross Technologies, Inc (Champaign, Illinois). As part of this effort, a fully functional and robust EMI/EMC analysis tool together with a functional interface will be developed to AFRL and subsequently commercialized. The development of this solver would have been impossible without the MURI effort.

III PERSONNEL RELATED TO MURI ACTIVITIES

University of Illinois at Chicago

Faculty

Uslenghi, Piergiorgio, PI
Dutt, Shantanu
Erricolo, Danilo
Yang, Hung-Yu

Graduate students (18)

Arslan, Hasan
Berardi, Cristian
Greenenwald. Kari
Kollman, Ronald
Larsen, Todd
Liang, Jing
Negri, Davide
Pellegrino, Paolo
Pincenti, John
Rota, Federico
Sahiti, Krishna
Sing, Pratibha
Sridhara, Sriramgopal
Stoia, Timothy
Tan, Qiwu
Trovò, Franco
Valentino, Marco
Zhou, Chengzhi

Clemson University

Faculty

Bridgwood, Michael A.
Butler, Chalmers M.
Martin, Anthony Q.
Tesche, Frederick M.

Graduate students (11)

Bopp, Charles L., III
Frye, Michael
Keen, Jason M.
Kondru, Dinakar
Lockard. Michael D.
Long, Robert
Potluri, Pramod
Ramani, Vivek
Screiber, Adam
Seerama, Chaitanya
Young, John C.

University of Houston
Faculty
Capolino, Filippo
Jackson, David R.
Wilton Donald R.
Graduate students (2)
Khayat, Michael
Lertsirimit, Chatrpol

University of Illinois at Urbana-Champaign
Faculty
Cangellaris, Andreas
Michielssen, Ericfv
Postdoctoral fellows
Lomakin, Vitaliy
Shen, Guoqiang
Graduate students (10)
Andriulli, Francesco
Bagci, Hakan
Choi, Myoung Joon
Ihm, Jae-Yong
Kemal, Aygun
Lu, Mingyu
Manetas, Giorgos
Moon, Se-Jung
Wu, Hong
Yilmaz, Ali

University of Michigan / Ohio State University
Faculty
Liepa, Valdis V.
Mazumder, Pinaki
Volakis, John L.
Graduate students (6)
Bayram, Yakup
Khan, Z.
Siah, EngSwee
Usner, Brian
Wang, Baouha
Yang, Taesik

IV DISTRIBUTION OF SCIENTIFIC RESULTS

A special issue of the Electromagnetics Journal contains some of the scientific results produced by this team of researchers. The special issues consisted of three numbers: Vol. 25, no.7-8, Oct-Dec. 2005, and Vol. 26, No. 1, Jan. 2006.

In addition to presentations at various international conferences, special sessions dedicated to this MURI were organized at:

1. IEEE Antennas and propagation Society International Symposia (2002 [20-33], 2003[41-77], 2004 [100-111], 2005 [126-135])
2. Boulder meeting (2002 [3-15], 2004 [84-93], 2005 [116-124], 2006 [144-150])
3. URSI EMTS Symposium in Pisa, 2004 [95-98]

Finally, a monograph entitled "Electromagnetic Interference in Complex Systems" will be published, probably by IEEE/Wiley Press.

LIST OF PRESENTATIONS AND PUBLICATIONS SUPPORTED BY THE U.S. DEPARTMENT OF DEFENSE UNDER MURI GRANT F49620-01-1-0436.

International Conference on Electromagnetics in Advanced Applications, September 1-14, 2001, Torino, Italy.

1. **P.L.E. Uslenghi,** ***Special solutions for isorefractive wedges***
2. **K. Aygün, B. Shanker, E. Michielssen ,** ***Low Frequency Plane Wave Time Domain Kernels***

National Radio Science Meeting, University of Colorado at Boulder , January 9-12,2002 , Boulder , CO , USA .

3. **P.L.E. Uslenghi,** ***Radiation, penetration and scattering for a slotted semielliptical channel filled with isorefractive material – I. Exact solutions***
4. **D. Erricolo, K.A. Greenenwald, P.L.E. Uslenghi,** ***Radiation, penetration and scattering for a slotted semielliptical channel filled with isorefractive material – II. Numerical results***
5. **D. Erricolo, P.L.E. Uslenghi,** ***Exact scattering from metallic wedges edge-coated with anisotropic materials***
6. **C.M. Butler, M.K. Lockard,** ***Penetration into and radiation from a slotted semielliptical channel filled with isorefractive material – Integral equation formulation and solution***
7. **M.G. Harrison, C.M. Butler, J.C. Young,** ***Analysis of signals in coupled coaxial and cylindrical cavities***
8. **A.Q. Martin,** ***On the effects of propagation path on RF signals in systems***
9. **F.M. Tesche, C.M. Butler,** ***Extension of the BLT equation to incorporate electromagnetic field propagation***
10. **C.M. Butler,** ***Some difficulties in aperture theory***
11. **E. Siah, K. Sertel, J.L. Volakis, V. Liepa,** ***EM coupling through slots into overmoded cavities and large scaled complex platforms using the multilevel fast multipole method***
12. **D.R. Wilton, D.R. Jackson, C. Lertsirimit,** ***Coupling of electromagnetic field to a wire in a cavity***
13. **K. Aygun, B. Fischer, A. Cangellaris, E. Michielssen,** ***Fast time domain analysis of nonlinearly loaded printed circuit board structures***
14. **M.A. Bridgwood,** ***Assessment of semiconductor non-linear loads via single-shot high voltage time domain reflectometry***
15. **S. Dutt, H. Arslan,** ***Evaluation of processor faults due to EM interference-concepts and simulation environment***

2002 Design, Automation and Test in Europe Conference and Exposition (DATE 2002), March 4-8, 2002 , Paris , France

16. **L. Ding, P. Mazumder,** ***Accurate Estimating Simultaneous Switching Noises by Using Application Specific Device Modeling***

52nd Electronic Components and Technology, May 28-31, 2002

17. **M.J. Choi and A.C. Cangellaris,** ***Efficient modeling and simulation environment for expedient preliminary design of complex power distribution networks***
18. **T.V. Yioultsis and A.C. Cangellaris,** ***Optimal synthesis of finite difference models for multiconductor transmission lines via Gaussian spectral rules***

Amerem, 2-7June 2002, Annapolis , Ma , USA

19. **D. Erricolo, P.L.E. Uslenghi,** ***Exact radiation from a line source in the presence of a ditch in a corner***

IEEE Antennas and Propagation Society International Symposium and United States National Council(USNC)/International Union of Radio Science (URSI) National Radio Science Meeting, June 16-21, 2002, San Antonio, Tx, USA

20. **D. Lockard, C. M. Butler,** ***Penetration through an Aperture Backed by a Channel --Integral Equation Formulation and Solution***
21. **E.S. Siah, T. Yang, K. Sertel and J.L. Volakis,** ***Electromagnetic analysis and shielding of slots on resonant and non- resonant realistic structures with MLFMM***
22. **D. Erricolo, P.L.E. Uslenghi,** ***Exact radiation from an antenna on a metal post at the interface between isorefractive half-spaces***
23. **J.C. Young, C.M. Butler, C.L. Bopp, III,** ***Transient Signals in Coupled Coaxial and Cylindrical Cavities***
24. **H.Y.D. Yang, L. Zhang,** ***Analysis of conducting EMI on radio-frequency integrated circuits***
25. **A. Rong, J. Morsey, K. Aygun, B. Fisher, E. Michielssen and A.C. Cangellaris,** ***Comparison of Two Methodologies for the Analysis of Distributed Integrated Circuits with Non-linear Driver/Receiver Electronics***
26. **E.S. Siah, J.L. Volakis and P.Y. Papalambros,** ***Parameter Optimization Using the Divided Rectangles Global Algorithm with Kriging Interpolation Surrogate Modeling***
27. **M. Lu and E. Michielssen,** ***Closed Form Evaluation of Time Domain Fields Due to Rao-Wilton-Glisson Sources for Use in Marching-on-in-Time Based EFIE Solvers*****, Vol. 1, pp. 74-77.**
28. **D. Jiao, J. Jin, E. Michielssen and D. Riley,** ***Time-Domain Finite-Element Simulation of Three-Dimensional Scattering and Radiation Problems Using Perfectly Matched Layers*****, Vol. 2, pp. 158-161**
29. **D. Weile, N. Chen, B. Shanker and E. Michielssen,** ***An Accurate Time-Marching Solution Method for the Electric Field Integral Equation Using a Bandlimited Extrapolator*****, Vol. 2, pp. 162-165**
30. **A. Yilmaz, K. Aygun, J. Jin and E. Michielssen,** ***Matching Criteria and the Accuracy of Time Domain Adaptive Integral Method*****, Vol. 2, pp. 166-169**
31. **H. Bagci, A. Yilmaz, A. Cangellaris and E. Michielssen,** ***Efficient Broadband Analysis of Microwave Components*****, Vol. 2, pp. 170-173**
32. **G. Kobidze, B. Shanker and E. Michielssen,** ***A fast time domain integral equation based scheme for analyzing scattering from dispersive objects*****,Vol. 3, pp. 164-167**
33. **V.G. Daniele, P.L.E. Uslenghi,** ***"The isorefractive wedge revisited"***

XXVII General Assembly of the International Union of Radio Science (URSI), Maastricht, THe Nederlands, Aug. 17-24, 2002

34. **J.C. Young and C.M. Butler,** ***"Efficient Analysis of a Thin-Wire Antenna Attached to a Body", p. 1397***

IEEE International Symposium on Electromagnetic Compatibility, Aug. 19-23,2002, Minneapolis, MN, USA

35. E.S. Siah, K. Sertel, J.L. Volakis, V. Liepa, *EM Coupling and suppression through slots into lossless overmoded cavities using the Multilevel Fast Multipole Algorithm*

16th IEEE International Conference on VLSI design, Jan. 4-8, 2003, New Delhi, India

36. L. Ding, P. Mazumder, *The Impact of Bit-Line Coupling and Ground Bounce on CMOS SRAM Performance*

IEEE International Symposium on Electromagnetic Compatibility, May 11-16, 2003, Istanbul, Turkey.

37. E.S. Siah, K. Sertel, R.W. Kindt, J.L. Volakis and V.V. Liepa, *Fast Frequency Domain Computational EM tools for System Analysis of EMI/EMC topologies*
38. E.S. Siah, T. Ozdemir, J.L. Volakis, P.Y. Papalambros and R.W. Wiese, Optimization for RF Coupling and Interference Reduction of Devices in Complex Systems (received the Best Paper Award)

IEEE International Symposium on Circuits and Systems, May 25-28, 2003, Bangkok, Thailand.

39. B. Wang, P. Mazumder, *Subgridding method for speeding up FD-TLM circuit simulation*
40. Q. Xu, P. Mazumder, *Efficient interconnect modeling by finite difference quadrature method*

IEEE International Antennas and Propagation Symposium and USNC/CNC/URSI North American Radio Science Meeting, June 22-27, 2003, Columbus, OH, USA.

41. J. Young, C.M. Butler, Analysis of a Coaxial Cavity with Cross-section Dependent Upon Axial Displacement
42. C. Bopp III, C.M. Butler, *Field in a Complex Cylindrical/coaxial Cavity Subject To Time-harmonic and Transient Excitation*
43. C. Bopp III, C.M. Butler, *Analysis of Transmission of a Signal Through a Complex Cylindrical/coaxial Cavity by Transmission Line Network Methods*
44. J. Young, C.M. Butler, Wire Antenna Attached To a Conducting Body and Coupled To an Enclosed Cavity
45. M. Lockard, C.M. Butler, *Penetration Through an Aperture Backed by a Channel - Coupled Integral Equation Formulation with Specific Green's Functions*
46. A. Martin, V. Ramani, C. Seerama, Effects of Propagation Path on Transient Signals in Electronic Systems
47. D. Negri, D. Erricolo, P.L.E. Uslenghi, Aperture Excitation of a Transmission Line in a Cavity
48. T. Yang, T. Ozdemir, E. Siah, J.L. Volakis, Network Analysis of Multiple Apertures on Cavity Enclosures with Wire Penetrations
49. D.R. Jackson, D.R. Wilton, C. Lertsirimit, Coupling To a Printed Circuit Board Inside a Cavity from a Wire Penetrating an Aperture
50. E. Siah, R.W. Kindt, K. Sertel, J.L. Volakis, Generalized FE-BI for Solving Mixed Surface and Volume Geometries
51. R. Kollman, H. Yang, *Susceptibility Analysis of a Cavity with an Aperture and System Effects*
52. J. Pincenti, P. Uslenghi, *EMI Coupling To Cable Bundles*
53. Y. Bayram, T. Ozdemir, J.L. Volakis, Coupling Among Multi-Conductor Transmission Lines

and Complex Structures

54. D. Erricolo, M. Lockard, C. Butler, P.L.E. Uslenghi, Analytical Formulas and Integral Equation Methods: a Study of Penetration, Radiation, and Scattering for a Slotted Semielliptical Channel Filled with isorefractive material
55. C. Berardi, D. Erricolo, P.L.E. Uslenghi, *Exact Analysis of a 3D Cavity-backed Aperture with an Isorefractive Lens*
56. J. Brunett, V. Liepa , *Broadband Antenna System for Uniform Field Generation*
57. E.S. Siah, J.L. Volakis, D. Pavlidis, V.V. Liepa, Plane Wave Illumination Effects onto Circuit Topologies
58. H. Yang, *Conducting EMI Effects on RF Active Circuits*
59. J. Meng, K. Aygun, E. Michielssen, *An Improved Fast Algorithm for Transient Simulation of Microwave Circuits with Nonlinear Electronics*
60. J. Morsey, M. Choi, V. Okhmatovski, A. Cangellaris, *A Hybrid Methodology for Efficient Electromagnetic Interference Modeling of High-density Printed Circuit Board*
61. Trovò, S. Dutt, H. Arslan, *Design and Simulation of an EM- Fault-Tolerant Processor with Micro-Rollback, Control-Flow Checking and ECC*
62. E.S. Siah, T. Ozdemir, J.L. Volakis, P.Y. Papalambros and R.W. Wiese, *Fast Parameter Optimization Using Kriging Macro-Modeling*
63. J.C. Young, *Novel method for the analysis of an antenna attached to a planar surface of a conducting body*
64. N. Chen, M. Lu, B. Shanker, and E. Michielsen, *Fast Integral-Equation-Based Analysis of Transient Scattering from Doubly Periodic Perfectly Conducting Structures*, pp.710.
65. J. Gao, B. Shanker, D.S. Weile, and E. Michielssen, *Analysis of Transient Scattering from Multiregion Bodies Using the Plane Wave Time Domain Algorithm*, pp.631
66. A. Boag, and E. Michielssen, *Multilevel Non-uniform Grid Algorithm for Fast Iterative Solution of Scattering Problems*, pp.652
67. A. Boag, E. Michielssen, V. Lomakin, and E. Heyman, *Non-uniform Grid Time Domain Approach For Fast Multilevel Evaluation of Transient Fields*, pp.709
68. A.E. Yilmaz, B. Shanker, J.M. Jin, and E. Michielssen, *Efficient Solution of Time Domain Volume Integral Equations using the Adaptive Integral Method*, pp.711
69. A.E. Yilmaz, J. Jin, and E. Michielssen, *Discrete Wavelet Transform Compression for Time Domain Integral Equations*, pp.712
70. N. Liu, M. Lu, A.E. Yilmaz, K. Aygun, B. Shanker, and E. Michielssen, *A Parallel Marching on in Time Solver Accelerated by Plane Wave Time Domain Algorithm*, pp.713
71. A.E. Yilmaz, J.M. Jin, and E. Michielssen, *Time Domain Adaptive Integral Method for the Combined Field Integral Equation*, Vol. 3, pp.543-546,.
72. P. Jiang, K. Yegin, S. Li, B. Shanker, and E. Michielssen, *An Improved Plane Wave Time Domain Algorithm for Dissipative Media*, vol. 3, pp.563-566
73. H. Bagci, A.E. Yilmaz, V. Lomakin, E. Michielssen, *Fast and Accurate Solution of Time Domain Electric Field Integral Equation for Dielectric Half-Space*, vol. 3, pp.583-586
74. V. Lomakin, N.W. Chen, and E. Michielssen, *Enhanced Transmission Through Periodic Subwavelength Hole Structures*, vol. 2, pp.821-824
75. G. Kobidze, B. Shanker, and E. Michielssen, *Hybrid PO-PWTD Scheme for Analyzing of Scattering from Electrically Large PEC Objects*, Vol. 3, pp547-550
76. R.D. Kollman and H.Y.D. Yang, *EMI Effect on active circuits*
77. P.L.E. Uslenghi, *"Introduction to EMI effects on complex platforms"*

5th International Congress on Industrial and Applied Mathematics, Sydney, Australia, July 2003

78. P.L.E. Uslenghi, *"Exact solutions for boundary-value problems involving isorefractive media"*

European Conference on Circuit Theory and Design, Sept. 1-4, 2003 , Krakow , Poland

79. **Q. Xu, P. Mazumder, *Modeling of Transmission Lines with EM Wave Coupling by Finite Difference Quadrature Methods***

International Conference on Electromagnetics in Advanced Applications, September 8-12, 2003, Torino, Italy.

80. **D. Erricolo, P.L.E. Uslenghi, *Exact scattering from a cylindrically-capped metallic wedge edge-coated with anisotropic material***
81. **D. Erricolo, M.D. Lockard, C.M. Butler, P.L.E. Uslenghi, *Comparison among currents on surfaces inside and near a semielliptical channel filled with isorefractive material that backs a slotted plane: currents computed by analytical formulas and by integral equation methods* <! [endif]>**

Progress in Electromagnetics Research Symposium (PIERS 2003), Honolulu, Hawaii, October 2003

82. **P.L.E. Uslenghi, "*Exact scattering by penetrable wedges*"**

IEEE/ACM International Conference on Computer-Aided Design, November 9-13, 2003

83. **T. Yioultsis, A. Woo, and A. C. Cangellaris, "*Passive synthesis of compact frequency-dependent interconnect models via quadrature spectral rules*"**

National Radio Science Meeting, University of Colorado at Boulder , January 5-8, 2004 , Boulder , Colorado , USA .

84. **D.R. Wilton, D.R. Jackson, W.A. Johnson, M.A. Khayat, and C. Lertsirimit, "*Validation as a Process,*" (Abstracts, p.63).**
85. **M.D. Lockard, C.M. Butler, "*Penetration through a slot in a conducting plane backed by a conducting channel,*", Student Paper Competition, (Full length paper.)**
86. **C.L. Bopp, III, and C.M. Butler, "*Field in a complex cylindrical/coaxial cavity subject to time-harmonic and transient excitation,*" Student Paper Competition (Full length paper.)**
87. **C.L. Bopp, III, and C.M. Butler, "*Response of a complex cylindrical/coaxial cavity subject to transient excitations*"**
88. **C.M. Butler, M.D. Lockard, "*Validation of integral equation methods: penetration through a slot in a conducting plane backed by a channel*"**
89. **E.S. Siah, J.L. Volakis and. Liepa, "*Validation of Transfer Function measurements for Analyzing Coupling of External Illumination to Circuit Elements within Metallic Enclosures*"**
90. **D. Erricolo, P.L.E. Uslenghi, "*Electromagnetic behavior of a partially covered trench in a corner*"**
91. **T. Larsen, D. Erricolo, P.L.E. Uslenghi, "*Low-frequency behavior of a slotted semielliptical channel*"**
92. **D. Erricolo, P.L.E. Uslenghi, "*Radiation and scattering for elliptic metal cylinder between isorefractive half-spaces*"**
93. **J.C. Pincenti, P.L.E. Uslenghi, *"Randomly-oriented nonuniform multiconductor transmission lines"***

International Symposium on Circuits and Systems, May 2004, Vancouver , British Columbia , Canada .

94. **B. Wang, P. Mazumder, "*Fast thermal analysis for VLSI circuits via semi-analytical Green's function in multi-layer materials*"**

URSI Intl. Symp. on Electromagnetic Theory, May 24-27, 2004, Pisa, Italy.

95. **C. Lertsirimit, D.R. Jackson, and D.R. Wilton, "*EMI Coupling to a Device on a Printed Circuit Board Inside a Cavity From a Wire Penetrating an Aperture*," pp. 816-818.**
96. **D. Erricolo, P.L.E. Uslenghi, "*Exact scattering from a cylindrically-capped metallic wedge edge-capped with anisotropic material: line source incidence*", pp. 120-122.**
97. **Q. Tan, D. Erricolo, P.L.E. Uslenghi , "*Eigenfunction solutions of radiation and scattering from a prolate spheroid with anisotropic surface impedance*", pp. 126-128.**
98. **D. Erricolo, P.L.E. Uslenghi, "*Radiation from a line source inside a trench in a corner*", pp. 813-815.**

Proc. 2004 Electronic Components and Technology Conference (ECTC'04), vol. 1, pp. 231-236, Jun. 2004.

99. **H. Wu and A.C. Cangellaris, "*Finite element analysis of passive electromagnetic devices including electrical circuit models*"**

IEEE International Antennas and Propagation Symposium and USNC/CNC/URSI National Radio Science Meeting, June 20-25, 2004, Monterey, California, USA.

100. **C. Lertsirimit, D.R. Jackson, D.R. Wilton, D. Erricolo, D.H.Y. Yang, "*Simulation and validation of EMI coupling to a circuit board from a wire penetrating a cavity enclosure*"**
101. **T.Yang, J.L. Volakis, "*Coupling to Wires in Cavity Enclosure using Iterative Algorithm*"**
102. **Y. Bayram, J.L. Volakis, "*Field Coupling Analysis of Multiconductor Transmission Lines in Presence of Complex Platforms via a Hybrid MoM-SPICE Technique*"**
103. **V. Ramani, A.Q Martin, "*A Study of Wideband Signal Propagation thru Cascaded Rectangular Cavities: Efficient Modeling using Matrix Interpolation Techniques*'**
104. **C. Sreerama, A.Q Martin, "On the use of extrapolation methods to assess the effects of propagation path on signals penetrating electronic systems due to HPM sources"**
105. **D. Negri, D. Erricolo, P.L.E. Uslenghi, "Penetration Into Nested Cavities Through Apertures"**
106. **A.E. Yilmaz, A.C. Cangellaris, J.-M. Jin, E. Michielssen, "*Time Domain Adaptive Integral Method for EMI/EMC Applications*"**
107. **M.D. Lockard, C.M. Butler, "*Penetration through a Slot in a Conducting Plane Backed by a Channel, Part II: TM Excitation*"**
108. **D. Erricolo, P.L.E. Uslenghi, "*Radiation from an antenna in a partially covered cavity near a 2D or 3D Corner*"**
109. **J.C. Pincenti, P.L.E. Uslenghi, "*Incident Field Excitation of a Random Two-Wire Transmission Line*"**
110. **M.A. Bridgwood, "*Susceptibility of digital IC's to ringing EMI events*"**
111. **P. Mazumder, B. Wang, "*Effects of External EMI Pulses on Microprocessor Instruction Execution*"**

EuroEM 2004, Euro Electromagnetics, 12-16 July 2004, Magdeburg , Germany

112. **J.C. Pincenti, P.L.E. Uslenghi, "*Incident field excitation of a random two-wire transmission line***

above a lossy ground plane", p. 99

113. **D. Negri, D. Erricolo, P.L.E. Uslenghi, "*Penetration into nested cavities through apertures*", p. 99**

IEEE International Symposium on Low Power Electronics Design, August 2004, Newport Beach , California , USA

114. **B. Wang, P. Mazumder, "*On optimality of adiabatic switching in MOS energy recovery circuit*"**

2004 IEEE Topical Meeting on Electrical Performance of Electronic Packaging (EPEP'04), Portland, Oregon, Oct. 2004.

115. **I.J. Chung and A.C. Cangellaris, "*Expedient methodology for the quantification of interconnect-induced semiconductor substrate noise*"**

National Radio Science Meeting, University of Colorado at Boulder , January 5-8, 2005 , Boulder, Colorado, USA .

116. **Y. Bayram, Z.A. Khan and J.L. Volakis, "*Experimental and Theoretical Study of Digital Circuits Subject to Electromagnetic Interference*"**
117. **S. Rahman, B. Elnour, D. Erricolo, P.L.E. Uslenghi, "*Measurements and theoretical results for the scattering by a ridge on a metal plane*"**
118. **C. Lertsirimit, D.R. Jackson, D.R. Wilton, D. Erricolo, "Time-domain coupling to a device on a printed circuit board inside a cavity"**
119. **Y. Bayram, Z.Khan and J. L. Volakis, "*Experimental and Theoretical Study of Digital Circuits Subject to Electromagnetic Interference*"**
120. **S. Oroskar, D. R. Jackson, and D. R. Wilton, "*The Best Choice of the Splitting Parameter in the Ewald Method*,"**
121. **H.Y.D. Yang and R.D. Kollman, "*Analysis of high-power RF Interference on digital circuits*"**
122. **C.L. Bopp, III, C.M. Butler, and F.M. Tesche, "*Coupling to a thin wire in a cylindrical/ coaxial cavity*"**
123. **C.L. Bopp, III, and C.M. Butler, "*Analysis of a pec hemisphere backed circular aperture excited by an axially directed dipole*"**
124. **J.C. Pincenti, P.L.E. Uslenghi, "*Incident field excitation of a random multiconductor transmission line in a corner formed by conducting walls*"**

IEEE VLSI Design International Conference, 3-7 January 2005, Taj Bengal , Kolkata , India

125. **B. Wang, P. Mazumder, "*Multivariate normal distribution based statistical timing analysis using global projection and local expansion*"**

IEEE AP-S International Symposium and USNC/URSI National Radio Science Meeting, 3-8 July 2005, Washington D.C., USA

126. **C.M. Butler, C.L. Bopp, III, D. Erricolo, M.D. Lockard, "*An Integral Equation with a Kernel***

***Expanded in Eigenfunctions for the Current on a Cylinder in an Elliptic Channel Excited through a Slot*"**

127. **C. Lertsirimit, D.R. Jackson, D.R. Wilton, D. Erricolo,** ***Transient Coupling to a Device on a Printed Circuit Board Inside a Cavity***
128. **D. Erricolo, P.L.E. Uslenghi, "*Exact Analysis of a 2D Cavity-backed Slot in a Ground Plane Covered by an Isorefractive Lens*"**
129. **Z.A. Khan,Y. Bayram, J.L. Volakis, "*EM Coupling to Cable Bundles in Shielding Cavities Using a Semi-Analytical Iterative Approach*"**
130. **T.Yang and J.L. Volakis, "*EMI Effects on Printed Circuit Boards Enclosed within Multilayer Cavities with Apertures*"**
131. **Y. Bayram and J.L. Volakis, "*Hybrid S-Parameters for Analysis of Mixed RF-Digital Circuits Subject to External Electromagnetic Interference*"**
132. **R.D. Kollman and H.Y.D. Yang, "*External EMI Effects on a CMOS Circuit in a Cavity with an Aperture*"**
133. **A.E. Yilmaz, M.J. Choi, A.C. Cangellaris, J.-M. Jin and E. Michielssen, "*Incorporation of frequency-dependent multipart macromodels into a fast time-domain integral equation solver*"**
134. **C.L. Bopp, III, and C.M. Butler, "*Coupling to a loaded thin wire in a cylindrical/ coaxial cavity*"**
135. **J. Liang, P.L.E. Uslenghi, "*Exact geometrical optics scattering by an isorefractive paraboloidal radome*"**

7th Biennial Engineering Mathematics and Applications Conference, Melbourne, Australia, September 2005

136. **P.L.E. Uslenghi, "*Exact solutions of electromagnetic boundary-value problems involving isorefractive materials*"**

IEEE EMC International Symposium, August 2005, Chicago, IL, USA

137. **Y. Bayram and J.L. Volakis, "*A Hybrid MoM-SPICE Technique For Field Coupling Analysis of Transmission Lines in Presence of Complex Structures*"**
138. **Y. Bayram and J.L. Volakis, "*A Novel Technique for Concurrent On & Off Board EMI Analysis of Mixed RF-Digital Circuits via Hybrid Scattering Parameters*"**
139. **A.C. Cangellaris and H. Wu, "*Domain decomposition and multi-scale finite elements for electromagnetic analysis of integrated electronic systems*"**

The Second LASTED International Conference on Antennas, Radar, and Wave Propagation, ARP 2005, July 19-21, Banff, Alberta, Canada

140. **D. Erricolo, P.L.E. Uslenghi, B. Elnour, "*Line source scattering by a ridge on a metal plane*"**

International Conference on Electromagnetics in Advanced Applications, Sept 12-16, 2005, Torino, Italy

141. **D. Erricolo, P.L.E. Uslenghi, M. Valentino, "*Exact Analysis of a Spheroidal Cavity with a Circular Aperture in a Ground Plane Covered by an Isorefractive Lens*"**

XXVIII General Assembly of the International Union of Radio Science, Oct. 23-29, 2005, New Delhi, India

142. **J.L. Volakis and Y. Bayram, "*EMI/EMC Characterization of Mixed Radio Frequency-Digital***

Circuits"

143. **C. Lertsirimit, D.R. Jackson, D.R. Wilton, D. Erricolo, "*Coupling to a Device on a Printed Circuit Board Inside of a Cavity*"**

National Radio Science Meeting, University of Colorado at Boulder , January, 2006 , Boulder , Colorado , USA .

144. **A.W. Schreiber, C.M. Butler, D. Erricolo, "*Current on a conducting cylinder in an elliptic channel excited through a slot in a conducting screen by an incident field TE to the slot axis*"**
145. **F.M. Tesche, C.M. Butler, A. Schreiber, and D.V. Giri, "*Estimates of the Near Field EM Environment of a Pyramidal Horn Antenna, with Applications to Vulnerability Testing of Common Electrical Appliances*"**
146. **Z.A. Khan, Y. Bayram, J.L. Volakis, "*Experimental Study of Electromagnetic Interference (EMI) on PCBs and Cables enclosed in Complex Structures*"**
147. **Y. Bayram, S.K. Myoung, S.J. Doo, P. Roblin and J.L. Volakis, "*Experimental and Theoretical Analysis of Digital Modulation Schemes and RF Power Amplifiers Subject to Electromagnetic Interference*"**
148. **C. Lertsirimit, D.R. Jackson, and D.R. Wilton, "*Efficient Techniques for the Calculation of EM Penetration into Cavities*"**
149. **C.L. Bopp, III, and C.M. Butler, "*Coupling of the field of an exterior monopole through an aperture in a pec screen to a loaded thin wire in a cylindrical/ coaxial cavity*"**
150. **J. Liang, P.L.E. Uslenghi, "Analytical and numerical study of multilayered paraboloidal radomes"**

Proc. 2006 IEEE MTT-S International Microwave Symposium, pp. 1609 – 1612, San Francisco, CA, Jun. 2006

151. **S.-J. Moon and A. C. Cangellaris, "*Rational function fitting of electromagnetic transfer functions from frequency-domain and time-domain data*"**
152. **H. Wu and A. Cangellaris, "*Krylov model order reduction of finite element models of electromagnetic structures with frequency-dependent material properties*"**

IEEE International Symposium Antennas and Propagation Society, 9-14 July 2006, Albuquerque, NM, USA

153. **T. Yang and J.L. Volakis, "*Aperture Coupling Method for EMI Analysis of Microwave Circuits within Multilayer Cavities*"**
154. **Z.A. Khan, J.L. Volakis, "*Experimental and Analytical Study of EMC/EMI effects on PCBs and Cables enclosed within metallic Enclosures*"**
155. **Y. Bayram, C. Chang, K. Kim, S.K. Myoung, S.J. Doo, P. Roblin, A. Iliadis and J.L. Volakis, "*Experimental and Theoretical Analysis of RF and Digital Systems in Presence of Complex Platforms Subject to Electromagnetic Interference*"**
156. **C.M. Butler, D. Erricolo, C.L. Bopp, III, A.W. Schreiber, "*Penetration Through a Slotted Screen into a Semi-Elliptic Channel: Simple Integral Equation with an Eigenseries Kernel*"**
157. **C.M. Butler, D. Erricolo, C.L. Bopp, III, A.W. Schreiber, "*Penetration Through a Slotted Screen into a Dielectric Cylinder Housed in a Semi-Elliptic Channel*"**
158. **F.M. Tesche and M.C. Miller, "*Development of the BLT Equation in the Time Domain for Transmission Line Networks*"**
159. **F.M. Tesche and P.F. Bertholet, "*Summary of EM Measurements of a Swiss Civil Defense Facility*"**
160. **D.V. Giri and F.M. Tesche, "*Classification and Examples of High-Power Electromagnetic***

(HPEM) Systems"

161. C.Z. Zhou and H.Y.D. Yang, "*External EMI reduction in high-frequency electronics systems using metamaterials*"
162. H.Y.D. Yang and C.Z. Zhou, "*The Reduction of electromagnetic interference in RF integrated circuits through the use of metalized substrates*"
163. A.W. Schreiber, C.M. Butler, F.M. Tesche, and D.V. Giri, "*Effects of high power electromagnetic radiation on electronic systems*"
164. P.L.E. Uslenghi, "*Exact geometrical optics scattering by some penetrable structures made of double-negative material*"
165. P.L.E. Uslenghi, "*Conditions for exact geometrical optics scattering by penetrable wedge structures*"

PIERS 2006, Tokyo, Japan, August 2006

166. P.L.E. Uslenghi, "*Canonical solutions for scattering by penetrable wedge structures*"
167. P.L.E. Uslenghi, "*Exact scattering by penetrable paraboloidal structures* "

2006 IEEE EMC International Symposium, Portland, OR

168. Y. Bayram, C.Chang, K. Kim, A. Iliadis and J.L. Volakis, "*High Power EMI on Digital Circuits within Automotive Structures*"
169. Z.A. Khan, Y. Bayram, J.L. Volakis, "*An Integrated Hybrid Solver and Measurements for EMI/EMC Analysis of Cables and PCBs Enclosed within Metallic Structures*"

21'st IEEE Int'l Symp. on Defect and Fault Tolerance in VLSI Systems (DFT'06)

170. F. Rota, S. Krishna and S. Dutt, "*Off-Chip Control Flow Checking of On-Chip Processor-Cache Instruction Stream*"

PUBLICATIONS IN REFEREED JOURNALS

171. D.V. Giri and F.M. Tesche, "*Classification of Intentional Electromagnetic Interference (IEMI)*", Special Issue on High Power Electromagnetic Fields, *IEEE Trans. on Electromagnetic Compatibility,* Vol. 46 (3),:Aug. 2003, pp. 322-328.

Analysis of pieces

172. E. Siah, K. Sertel, J.L. Volakis, V.V. Liepa, R.W. Wiese, "*Coupling Studies and shielding techniques for electromagnetic penetration through apertures on complex cavities and vehicular platforms*", *IEEE Trans. on Electromagnetic Compatibility*, Vol. 44, May 2003, pp. 245-256.
173. A.Q. Martin, C. Sreerama, "*The effects of transient signal propagation through electronic systems in FDTD*", *Technical Report*, Oct. 2004.
174. A.Q. Martin, V. Ramani, "*Propagation through wire-loaded cascaded rectangular cavities connected by narrow slots*", *Technical Report.*
175. C. Pincenti, P.L.E. Uslenghi, "*Incident field excitation of randomly oriented non uniform multiconductor transmission lines*", *IEEE Trans. Electromagnetic Compatibility,* submitted, 2003.
176. J.C. Young, C.M. Butler, and M.G. Harrison, "*Transmission Through Axisymmetric,*

Cascaded Cylindrical Cavities Coupled by Apertures - Part 1: Structures with Coaxial and Circular-Cylindrical Cross-Sections", *IEEE Trans. Electromagn. Compat.*, submitted, August 2002.

177. J.C. Young and C.M. Butler, "*Transmission Through Axisymmetric, Cascaded Cylindrical Cavities Coupled by Apertures - Part 2: Structures with Varying Cross-Sections*", *IEEE Trans. Electromagn. Compat.*, submitted, December 2002.
178. M.D. Lockard and C.M. Butler, "*Penetration through a slot in a conducting plane backed by a conducting channel, part I, TE case*", *IEEE Trans. on Antennas and Propagation*, submitted 2003.
179. F.M. Tesche, C.M. Butler, "*On the addition of EM field Propagation and Coupling effects in the BLT equation*", *Interaction Notes*, Note 588, June. 2004.
180. F.M. Tesche, J. Keen, C.M. Butler, "*Example of the use of the BLT equation for EM field propagation and coupling calculations*", *Interaction Notes*, Note 591, Aug. 2004.
181. C. Lertsirimit, D.R. Jackson, and D.R. Wilton, "*An Efficient Hybrid Method for Calculating the EMC Coupling to a Device on a Printed Circuit Board inside a Cavity by a Wire Penetrating an Aperture,*" *Electromagnetics,* submitted.
182. C. Lertsirimit, D.R. Jackson, and D.R. Wilton, "*Time-Domain Coupling to a Device on a Printed Circuit Board Inside a Cavity,*" *Radio Science*, submitted.
183. T. Yang and J.L. Volakis, "*Coupling onto Wires Enclosed in Cavities with Apertures*", *Electromagnetics Journal*, submitted.
184. F.M. Tesche and C.M. Butler, "*On the Addition of EM Field Propagation and Coupling Effects in the BLT Equation*", Interaction Note 588, Air Force Research Laboratory, Kirtland AFB, NM., December 13, 2003, Revised June 8, 2004
185. D.V. Giri , and F.M. Tesche, "*Classification of Intentional Electromagnetic Environments"* (IEME), IEEE Trans. EMC, Aug. 2004, Vol.46, No.3.
186. D.V. Giri, F. M. Tesche and C.E. Baum, "*An Overview of High-Power Electromagnetic (HPEM) Radiating and Conducting Systems*", Circuit and Electromagnetic System Design Notes (CESDN) Note 50, Air Force Research Laboratory, Kirtland AFB, NM., 24 February 2006.
187. F.M. Tesche, "*On the Analysis of a Transmission Line with Nonlinear Terminations using the Time Dependent BLT Equation*", IEEE Transactions on Electromagnetic Compatibility, submitted June 17, 2006
188. S. Oroskar, D.R. Jackson, and D.R. Wilton, "*The Optimum Choice of the Splitting Parameter in the Ewald Method,*" submitted to the Journal of Computational Physics.
189. J.C. Young, C.M. Butler, "*An efficient method for the analysis of a structure comprising an appendage attached to a planar surface of a conducting body*", IEEE Trans. Antennas Propagat., vol. 53, no.9, September 2005.
190. M.D. Lockard, C.M. Butler, "*Penetration through a slot in a conducting plane backed by a conducting-wall channel: Transverse electric case*", Radio Science, Vol. 39, No. 6, RS6011, 02 December 2004
191. M.D. Lockard, C.M. Butler, "*Penetration through a slot in a conducting plane backed by a conducting-wall: Transverse magnetic case*", Radio Science, reviewed, modified, and resubmitted, 2006
192. C.L., Bopp, III, and C.M. Butler, "*Efficient methods for Determining the Coupling to Wires in Circular Cavities*", IEEE Trans. Electromag. Compat., accepted.

DIGITAL/HIGHER COMPLEXITY SYSTEMS

193. H.-Y. D. Yang, "*Analysis of Radiation Interference on Wireless Communication Systems*", *IEEE Antennas and Wireless Propagation Letters*, 2003, pp.126-129.
194. M.A. Bridgwood, "*Susceptibility of digital IC's to conducted Ringing EMI*", *IEEE Trans on*

EMC., submitted 2003

195. S. Dutt, F. Rota, F. Trovo and F. Hanchek, "*Fault Tolerance in Computer Systems-From Circuits to Algorithms*", (invited article), in *Electrical Engineering Handbook*, Ed. Wai-Kai Chen, Academic Press, 2003.
196. L. Ding, P. Mazumder, "*Simultaneous Switching Noise Analysis Using Application Specific Device Modeling*", *IEEE Trans. on VLSI*, submitted, 2003.
197. H.Y. D. Yang and R.D. Kollman, "*Analysis of high-power RF Interference on digital circuits,*" Accepted for publications in *Electromagnetics, Special Issues on High-Power RF Interference*, Vol. 26, no. 1, pp. 87-100, January/February 2006.
198. H.Y.D Yang and C-Z Chou, "*On the use of vias loaded microstrips for size and cross-talk reduction in RFIC,*" Submitted to IEEE Transaction on Microwave Theory and Techniques, June 2006.

Development of large scale solvers

199. K. Aygün, B. Shanker, A. A. Ergin, E. Michielssen, "*A two-level plane wave time-domain algorithm for fast analysis of EMC/EMI problems*", *IEEE Trans. on Electromagnetic Compatibility*, Vol. 44(1), pp. 152-164, Feb. 2002.
200. M. Lu, B. Shanker, and E. Michielssen, "*Fast time domain integral equation solvers for analyzing two-dimensioanl scattering phenomena, Part II: full PWTD acceleration*", *Electromagnetics*, submitted, 2003.
201. Q. Chen, M. Lu, and E. Michielssen, "*Integral Equation Based Analysis of Transient Scattering from Surfaces with Impedance Boundary Condition,*" *Microwave and Optical Technology Letters*, vol. 42, no. 3, pp. 213-220, 2004.
202. A. Yilmaz, J. Jin, and E. Michielssen, "*Time domain adaptive integral method for surface integral equations,*" IEEE Trans. Antennas Propagat, vol. 52, pp. 2692-2708, 2004.
203. K. Aygün, B. Shanker, E. Michielssen, "*Fast Time domain Characterization of Finite Size Microstrip structures*" , *International Journal of Numerical Modeling*, submitted.
204. B. Shanker, K. Aygun, E. Michielssen, "*Fast analysis of transient scattering from lossy inhomogeneous dielectric bodies*", *Radio Science,* submitted, 2003.
205. M. Lu, K. Yegin, and E. Michielssen, "*Fast time domain integral equation solvers for analyzing two-dimensional scattering phenomena; Part 1: temporal acceleration,*" *Electromagnetics*, vol. 24, pp. 425-449, 2004.
206. M. Lu, B. Shanker, and E. Michielssen, "*Elimination of spurious solutions associated with exact transparent boundary conditions in FDTD solvers,*" *IEEE Antennas and Wireless Propagation Letters*, vol. 3, pp. 59-62, 2004.
207. M. Lu, M. Lv, A. Ergin, B. Shanker, and E. Michielssen, "*Multilevel plane wave time domain based global boundary kernels for two-dimensional finite difference time domain simulations*" *Radio Science*, to appear, 2004.
208. K. Aygun, B. C. Fischer, J. Meng, B. Shanker, and E. Michielssen, "*A fast hybrid field-circuit simulator for transient analysis of microwave circuits,*" *IEEE Transactions on Microwave Theory and Techniques*, vol. 52, pp. 573-583, 2004.
209. G. Kobidze, G. Jun, B. Shanker, E. Michielssen, "*A fast time domain integral equation based scheme for analyzing scattering from dispersive objects*", *IEEE Trans. Antennas Propagat.*, submitted
210. H. Bagci, A. Yilmaz, and E. Michielssen, "*Fast solution of mixed potential time domain integral equations for half-space environments*", *IEEE Transactions on Geoscience and Remote Sensing*, submitted, 2004.
211. N. Chen, M. Lu, F. Capolino, B. Shanker, and E. Michielssen, "*Floquet-wave-based analysis of transient scattering from doubly periodic, discretely planar, perfectly conducting objects*", *Radio Science*, submitted, 2004.

212. A. Yilmaz, J. Jin, and E. Michielssen, "*A parallel FFT-accelerated field-circuit simulator*", *IEEE Trans. Microwave Theory and Techniques*, submitted, 2004
213. E.S. Siah, K. Sertel, J.L. Volakis, V.V. Liepa, R.W. Wiese, "*Coupling Studies and shielding techniques for electromagnetic penetration through apertures on complex cavities and vehicular platforms*", *IEEE Trans. on Electromagnetic Compatibility*, Vol. 44, May 2003, pp. 245-256.
214. E.S. Siah, M. Sasena, J.L. Volakis, P.Y. Papalambros, R.W. Wiese, "*Fast Parameter Optimization of Large Scale Electromagnetic Objects using DIRECT with Kriging MetaModeling*", *IEEE Trans. on Microwave Theory and Techniques*, Vol. 52, No. 1, Jan. 2004, pp. 276-285.
215. Y. Bayram and J.L. Volakis, "*A Hybrid MoM-SPICE Technique for Field Coupling Analysis of Transmission Lines in Presence of Complex Structures*", *IEEE Trans. On Electromagnetic Compatibility,* submitted.
216. Y. Bayram and J.L. Volakis, "*A Generalized MoM-SPICE Iterative Technique for Field Coupling to Multi- Conductor Transmission Lines in Presence of Complex Structures*", *IEEE Trans. On Electromagnetic Compatibility,* accepted.
217. H. Wu and A.C. Cangellaris, "*Model-order reduction of finite-element approximations of passive electromagnetic devices including lumped electrical-circuit models*," IEEE Trans. Microwave Theory & Techniques, vol. 52, no. 9, pp. 2305-2313, Sep. 2004.

VALIDATION AND MEASUREMENTS

218. D. Erricolo, "*Acceleration of the convergence of series containing Mathieu functions using Shanks transformation*", *IEEE Antennas and Wireless Propagation Letters*, Vol. 2, 2003, pp.58-61
219. P.L.E. Uslenghi, "Exact Penetration, "*Radiation and Scattering for a Slotted Semielliptical Channel Filled with Isorefractive Material*", *IEEE Trans. on Antennas and Propagation", IEEE Trans. Antennas Propagat.*, Vol. 52(6), June 2004, pp. 1473-1480.
220. E.S. Siah, J.L. Volakis and D. Pavlidis, "*Electromagnetic Analysis of Plane Wave Illumination Effects onto Passive and Active Circuit Topologies*", *IEEE Antennas and Wireless Propagation Letters*, Vol. 2, 2003, pp. 230-233.
221. C. Berardi, D. Erricolo, P.L.E. Uslenghi, "*Exact dipole radiation for an oblate spheroidal cavity filled with isorefractive material and aperture-coupled to a half space*", *IEEE Trans. on Antennas and Propagation, IEEE Trans. Antennas Propagat.*, Vol. 52(9), Sept. 2004, pp. 2205-2213.
222. D. Erricolo, P.L.E. Uslenghi, "*Exact Radiation and Scattering for an Elliptic Metal Cylinder at the interface between Isorefractive Half-spaces*", *IEEE Trans. Antennas Propagat.*, Vol. 52(9), Sept. 2004, pp. 2214-2225.
223. P.L.E. Uslenghi, "*Exact Geometrical Optics Scattering From a tri-sector isorefractive wedge structure*", *IEEE Antennas and Wireless Propagation Letters*, Vol. 3, 2004, pp. 94-95.
224. P.L.E. Uslenghi, "*Exact geometrical optics scattering from a right-angle isorefractive wedge structure*", *IEEE Antennas and Wireless Propagation Letters*, Vol. 3, 2004, pp. 127-128
225. D. Erricolo, M.D. Lockard, C.M. Butler, P.L.E. Uslenghi , "*Currents on conducting surfaces of a semielliptical-channel-backed slotted screen in an isorefractive environment*", *IEEE Trans. on Antennas and Propagation*, Vol. 53, No. 7, July 2005, pp. 2350-2356
226. D. Erricolo, P.L.E. Uslenghi, "*Penetration, Radiation and Scattering for a Cavity-backed Gap in a Corner*", *IEEE Trans. Antennas Propagat.*, Vol. 5, No. 8, Aug 2005, pp. 2738-2748
227. D. Erricolo, M.D. Lockard, C.M. Butler, P.L.E. Uslenghi, "*Numerical analysis of penetration, radiation and scattering for a slotted semielliptical channel filled with isorefractive material*", *Progress in Electromagnetic Research (PIER),* Vol. 53, pp. 69-89, 2005.
228. D. Erricolo, P.L.E. Uslenghi, "*Exact radiation for dipoles on metallic spheroids at the interface between isorefractive half-spaces*", *IEEE Transactions on Antennas and Propagation,* , Vol. 53,

No. 12, pp. 3974-3981, Dec. 2005.

229. D. Erricolo, P.L.E. Uslenghi, B. Elnour, F. Mioc, "*Scattering by a blade on a metallic plane*", *Electromagnetics - Special Issue on RF Effects on Digital Systems,* Vol. 26, No. 1, 2006, pp. 57-72.
230. D. Erricolo, *"Algorithm 861: Fortran 90 Subroutines for Computing the Expansion Coefficients of Mathieu Functions using Blanch's Algorithm", Association for Computing Machinery Transactions on Mathematical Software, Vol. 32(4),Dec. 2006, pp. 622-634*
231. M. Valentino, D. Erricolo, *"Exact 2D scattering from a slot in a ground plane backed by a semielliptical cavity and covered with an isorefractive lens"*, to be submitted to Radio Science, July 2006.
232. M. Valentino, D. Erricolo, *"Exact 3D scattering from a circular aperture in a ground plane backed by a spheroidal cavity and covered with an isorefractive lens"*, to be submitted to Radio Science, July 2006.
233. P.L.E. Uslenghi, "*Exact geometrical optics scattering by a right-angle wedge made of double-negative material*", *IEEE Trans. Antennas Propagat.*, Vol. 54(8), Aug. 2006, pp. 2301-2304.
234. P.L.E. Uslenghi, "*Invisible trenches partially filled with metamaterials*", *IEEE Antennas Wireless Propagat. Letters,* in preparation.
235. P.L.E. Uslenghi, "*Exact transmission through a metamaterial paraboloidal radome*", in preparation.
236. J. Liang and P.L.E. Uslenghi, "*Exact geometrical optics scattering by isorefractive paraboloidal structures*", *IEEE Trans. Antennas Propagat.*, submitted for Special Issue in memory of L. B. Felsen.
237. V.G. Daniele and P.L.E. Uslenghi, "*The isorefractive wedge*", *Radio Science*, in preparation for Special Issue on Analytical Scattering.
238. P.L.E. Uslenghi, "*Metamaterial translators and rotators*", *IEEE Trans. Antennas Propagat.,* in preparation.